fire

MDPI

Article

Effects of Barium Carbonate and Barium Titanate Particle Additives on the Performance and Emissions of a Diesel Engine Fueled with an Olive Pomace Oil Biodiesel–Diesel Blend

İbrahim Gündüz [1,2], Fatma Oflaz [3] and Turan Gürgenç [3,*]

[1] Automotive Technology Program, Vocational School of Technical Sciences, Bingöl University, 12000 Bingöl, Türkiye; igunduz@bingol.edu.tr
[2] Graduate School of Natural and Applied Sciences (Automotive Engineering), Fırat University, 23119 Elazig, Türkiye
[3] Department of Automotive Engineering, Technology Faculty, Firat University, 23119 Elazig, Türkiye
* Correspondence: tgurgenc@firat.edu.tr

Abstract

Improving fuel efficiency while controlling exhaust emissions is important for the wider use of biodiesel blends. The effects of barium carbonate and barium titanate were compared using a base fuel composed of equal volumes of diesel and biodiesel derived from olive pomace oil. Each additive was evaluated at 25, 50, and 100 ppm, with diesel, untreated BP50, and neat biodiesel serving as reference fuels. Tests used a single-cylinder diesel engine operated at 2000 rpm over a brake power range of 1.0–3.0 kW. Performance, exhaust gas concentrations, smoke opacity, exhaust temperature, and sound pressure level were measured. For neat biodiesel, the largest increases relative to diesel were 24.52% in brake specific fuel consumption and 42.86% in nitrogen oxide concentration. At 2.0 kW, the formulations containing 50 ppm $BaCO_3$ and $BaTiO_3$ exhibited brake specific fuel consumption values 3.80% and 3.79% below that of BP50, respectively. Both formulations raised brake thermal efficiency from approximately 22.38% to 23.27%. Relative to BP50, maximum reductions were 44.32% in carbon monoxide concentration with 50 ppm $BaTiO_3$ at 2.5 kW, 40.00% in hydrocarbon concentration with 100 ppm $BaCO_3$ at 2.5 kW, and 31.25% in smoke opacity with 50 ppm $BaCO_3$ at 1.0 kW. However, NO_X concentrations increased by up to 19.87% with 100 ppm $BaTiO_3$ at 2.0 kW compared with BP50. Under the tested conditions, 50 ppm $BaCO_3$ provided a favorable balance among fuel consumption, smoke opacity, and sound pressure level, with a smaller NO_X increase than the corresponding $BaTiO_3$ formulation.

Keywords: olive pomace oil biodiesel; barium carbonate particles; barium titanate particles; diesel engine; exhaust emissions; particle-added biodiesel; sustainability

Check for updates

Academic Editors: Jiaqiang E and Mingzhang Pan

Received: 29 September 2026
Revised: 29 October 2026
Accepted: 2 November 2026
Published: 4 November 2026

Copyright: © 2026 by the authors. Licensee MDPI, Basel, Switzerland. This article is an open access article distributed under the terms and conditions of the Creative Commons Attribution (CC BY) license.

1. Introduction

Interest in biodiesel as a compression-ignition engine fuel has grown with efforts to replace petroleum resources with renewable energy sources [1,2]. Biodiesel combines renewability and biodegradability with an oxygenated composition and can be incorporated into conventional diesel blends [1,3]. Establishing its suitability for engine use also requires determining how it affects energy conversion and exhaust emissions [4]. Feedstock selection influences both the production cost and the sustainability of biodiesel. Potential competition between edible oil consumption and fuel manufacture has directed attention toward waste materials and feedstocks of limited economic value. Recovering oil retained in olive pomace

allows a byproduct of olive oil processing to be converted into biodiesel, adding value to this residual material [5,6]. Mehdi et al. [7] achieved an oil recovery yield of up to 12% from olive pomace after optimizing hexane extraction through a central composite experimental design and response surface analysis. Lama-Muñoz et al. [8] demonstrated that treating two-phase olive pomace with steam at 160 °C for 60 min increased the oil concentration in the recovered solid by approximately 50%. The extracted oil subsequently achieved a biodiesel yield of approximately 95% through acid esterification followed by alkaline transesterification, with comparable conversion yields for oils obtained from treated and untreated pomace. Using a sulfonated solid acid catalyst prepared from olive pomace, Ayadi et al. [9] esterified the recovered oil with methanol and reduced its acid value to less than 2 mg KOH g^{-1} within 5 h. In a separate study, Ayadi et al. [10] treated oil with an initial acid value of 126.39 mg KOH g^{-1} using a heterogeneous catalyst derived from pomace. Methanol treatment yielded a final acid value of 1.14 mg KOH g^{-1} compared with 3.89 mg KOH g^{-1} after ethanol treatment. Yücel [11] investigated an enzymatic approach to biodiesel production using olive pomace as an immobilization support for thermomyces lanuginosus lipase. Introducing methanol in three stages yielded up to 93% biodiesel from olive pomace oil after a 24 h reaction at 25 °C. The immobilized enzyme maintained its catalytic activity over ten consecutive reaction cycles. These investigations demonstrate complementary approaches to recovering the residual oil and converting it into biodiesel. Olive pomace methyl ester differs from diesel in several fuel properties. Compared with diesel, its reduced energy content can increase the fuel required for a given output, while greater density and viscosity may impair spray development. Its oxygen content can also support oxidation and reduce some incomplete combustion emissions [12,13]. Previous engine studies show that the behavior of olive pomace biodiesel depends on blend ratio and operating conditions [13,14]. López et al. [15] examined how imposing emission constraints changes fuel economy in diesel blends containing olive pomace oil methyl ester. Emission limits set at 10%, 20%, and 40% below the measured maxima yielded model predicted optimal brake specific fuel consumption values of 368.1, 372.1, and 381.6 g kW^{-1} h^{-1}, respectively. Under the least restrictive scenario, the optimum combined 63.95% olive pomace oil methyl ester with 60.3% engine load, illustrating how emission constraints influence both fuel selection and operating conditions. For the same methyl ester, the reported cloud, pour, and cold filter plugging points were −2, −6, and −9 °C, respectively, while oxidative stability reached 15.5 h at 110 °C. These measurements complement the engine results by characterizing resistance to oxidation and behavior at low temperatures, which require evaluation separately from combustion performance. Oxygenated liquid components offer an alternative approach to modifying diesel fuel emissions. Bereczky et al. [16] incorporated γ-valerolactone (GVL), a cyclic ester obtainable from biomass, into a ternary fuel comprising diesel, biodiesel, and GVL at volumetric proportions of 71.4%, 21.5%, and 7.1%, respectively. At full load, this formulation reduced average smoke concentration by 47% relative to neat diesel, compared with 23% for the diesel and biodiesel blend without GVL. CO and total unburned hydrocarbon emissions also decreased, particularly at full load, while NO_X concentrations remained broadly similar. All three fuels reached a maximum brake thermal efficiency of approximately 38.8%. At full load, the average brake specific fuel consumption of the GVL formulation exceeded that of diesel by 6.8%. Çaynak et al. [17] reported a 20.37% decrease in the viscosity of olive pomace oil methyl ester following manganese-based additive incorporation at 12 μmol L^{-1}. For the treated blend containing 25% biodiesel, peak torque was 181.7 N m at 1400 rpm and peak power was 39.8 kW at 2400 rpm. The corresponding diesel values were 184.7 N m and 39.9 kW. Using waste cooking palm oil biodiesel, Kannan et al. [18] assessed the catalytic use of ferric chloride by dosing biodiesel derived from waste cooking palm oil at 20 μmol L^{-1}. With engine speed

fixed at 1500 rpm and fuel injected at 280 bar and 25.5° before top dead center, the treated biodiesel produced 52.6% less CO, 26.6% less total hydrocarbon, and 6.9% less smoke than the untreated fuel. Zhen et al. [19] identified the main combustion noise component within the 2–3 kHz frequency band in an engine operating on rapeseed biodiesel. The extracted combustion noise sound pressure levels were slightly higher for B50 and B100 than for diesel, with B50 consistently producing the highest levels across the tested conditions. Adding nanoparticles to biodiesel formulations has been investigated as a way to address limitations in fuel utilization and exhaust quality. The resulting engine response varies with the particle material and dosage, the composition of the base fuel, and the conditions under which the engine operates [2,20,21]. Hosseini et al. [3] prepared B5 and B10 fuels from waste cooking oil biodiesel and evaluated Al_2O_3 additions of 30, 60, and 90 ppm. Their optimum formulation increased engine power and torque by 5.36% each relative to neat diesel, accompanied by a 10.63% improvement in brake thermal efficiency and a 14.66% reduction in specific fuel consumption. The emission response comprised reductions of 2.94% for CO and 20.56% for unburned hydrocarbons, together with a 43.61% rise in NO. Ghanbari et al. [22] examined diesel and biodiesel formulations, including B20, after incorporating carbon nanotubes or silver nanoparticles at 40, 80, and 120 ppm. Across the formulations containing particles, the largest decreases relative to neat diesel were 7.08% for brake specific fuel consumption and 25.17% for CO, whereas NO_X increased by as much as 25.32%. El-Seesy et al. [23] examined graphene nanoplatelets in a blend containing 20% jatropha methyl ester and 80% diesel. At graphene nanoplatelet dosages of 50–75 mg L^{-1}, brake specific fuel consumption was 20% lower and brake thermal efficiency was 25% higher than for the blend without nanoparticles. For additions of 25–50 mg L^{-1}, NO_X fell by 40%, CO by 60%, and unburned hydrocarbons by 50%. More recent work also shows that the response depends on both the nanoparticle and the biodiesel feedstock. Sekhar and Gupta [24] used a diesel blend containing 20% rapeseed biodiesel to compare CNT, Al_2O_3, and ZnO, each dosed at 50 ppm. At full load, the CNT blend combined a brake thermal efficiency of 35.76% with a brake specific fuel consumption of 0.16 kg Kw^{-1} h^{-1}. These were the most favorable performance values among the nanoparticle blends, although this formulation also produced the highest NO_X concentration. Gad et al. [25] compared B20 fuels derived from jatropha, waste cooking oil, and corn after incorporating CNTs at 25, 50, or 100 mg L^{-1}. At 100 mg L^{-1}, brake thermal efficiency increased by approximately 9%, 13% and 15% for the respective blends relative to their corresponding nanoparticle-free B20 fuels. These findings indicate that the response to a given nanoparticle concentration can differ with the biodiesel feedstock. Wu et al. [26] evaluated 30 ppm carbon-coated aluminum nanoparticles in a fuel containing 96% of a palm biodiesel–diesel B10 blend and 4% ethanol. Testing over the European Stationary Cycle showed 6% decreases in both average brake specific fuel consumption and NO_X emissions, together with a 19% decrease in CO, when this formulation replaced B10. Particle number emissions nevertheless increased, indicating that the fuel economy and gaseous emission benefits did not extend to all measured pollutants. Savaş et al. [27] investigated $MgCO_3$ nanoparticles in a 10% jojoba biodiesel–diesel blend. At 2.5 kW, the blend dosed at 50 ppm reached its maximum brake thermal efficiency of 31% and its minimum BSFC of 259.20 g Kw^{-1} h^{-1}. For the 100 ppm formulation, average HC emissions were 65.87% lower than for diesel, whereas NO_X emissions were 15.16% higher. Haq et al. [28] evaluated $BaTiO_3$ and MoS_2 at dosages of 50 and 100 ppm using C20, a fuel prepared from diesel and castor biodiesel in an 80:20 ratio. C20Ba100 showed the most favorable overall response among the tested formulations. For C20Ba100, the gain in brake thermal efficiency relative to diesel was 6.47%, accompanied by an 8.1% decrease in brake specific fuel consumption. The corresponding emission decreases were 37.7% for CO, 22.4% for HC, and 26% for NO_X. Canan et al. [29] reported that adding 50 ppm $BaTiO_3$ to

a diesel blend containing 10% Spirulina biodiesel yielded 22.8% brake thermal efficiency and 367.35 g Kw^{-1} h^{-1} brake specific fuel consumption at 2.5 kW. With 150 ppm, average CO emissions decreased by 22.2% relative to diesel. Their simultaneous optimization of multiple responses identified a dosage of 150 ppm and a brake power of 1361.85 W, for which the model predicted a brake thermal efficiency of 17.02% and a brake specific fuel consumption of 526.36 g Kw^{-1} h^{-1}.

Previous studies have investigated carbonate and titanate additives in biodiesel fuels, including $MgCO_3$ in jojoba biodiesel blends and BaTiO3 in castor and Spirulina biodiesel blends [27–29]. The present investigation extends these comparisons to BP50, prepared from equal volumes of diesel and olive pomace oil biodiesel, by evaluating separate additions of submicrometre $BaCO_3$ particles and $BaTiO_3$ nanoparticles at 25, 50, and 100 ppm. The experimental design includes D100, additive-free BP50 and BP100 alongside the six particle-containing formulations. Comparing BP50 and BP100 with D100 characterizes the changes associated with biodiesel substitution, while comparisons against additive-free BP50 distinguish the additional effects of particle incorporation without altering the biodiesel fraction. The nine fuel formulations were tested at 2000 rpm over five brake power settings between 1 and 3 kW, providing matched operating points for comparing the two additives at each dosage. BTE and BSFC are evaluated together with CO, HC, CO_2 and NO_X concentrations, smoke opacity, EGT and A-weighted sound pressure level. The contribution is the comparative assessment of the concentration- and load-dependent benefits and limitations of these two particle formulations in a common waste-derived fuel. Because the two powders differ in both chemical composition and nominal particle size, the comparison evaluates the supplied formulations without isolating the contribution of either characteristic. This assessment examines whether improvements in fuel utilization and incomplete combustion indicators are accompanied by adverse changes in other measured responses, while distinguishing improvements over BP50 from performance relative to conventional diesel.

2. Materials and Methods

2.1. Biodiesel Production from Pomace Oil

Figure 1 outlines the alkaline transesterification route used to convert olive pomace oil into its methyl ester. The volumetric ratio of olive pomace oil to methanol was set at 5:1, and sodium hydroxide was used as the alkaline catalyst at a concentration of 5 g per liter of olive pomace oil. Complete dissolution of sodium hydroxide in methanol preceded the addition of the resulting sodium methoxide solution to the olive pomace oil. Throughout the 2 h reaction, the mixture was maintained at 60 °C and stirred continuously at 600 rpm. The reacted mixture was allowed to settle in a separating funnel for approximately 12 h without agitation. The lower layer, which was rich in glycerol, was removed to retain the upper methyl ester phase. The crude methyl ester underwent water washing to remove residual methanol, catalyst, glycerol, and other impurities. The washed product was subsequently heated to 110 °C to evaporate residual water and obtain purified olive pomace oil methyl ester.

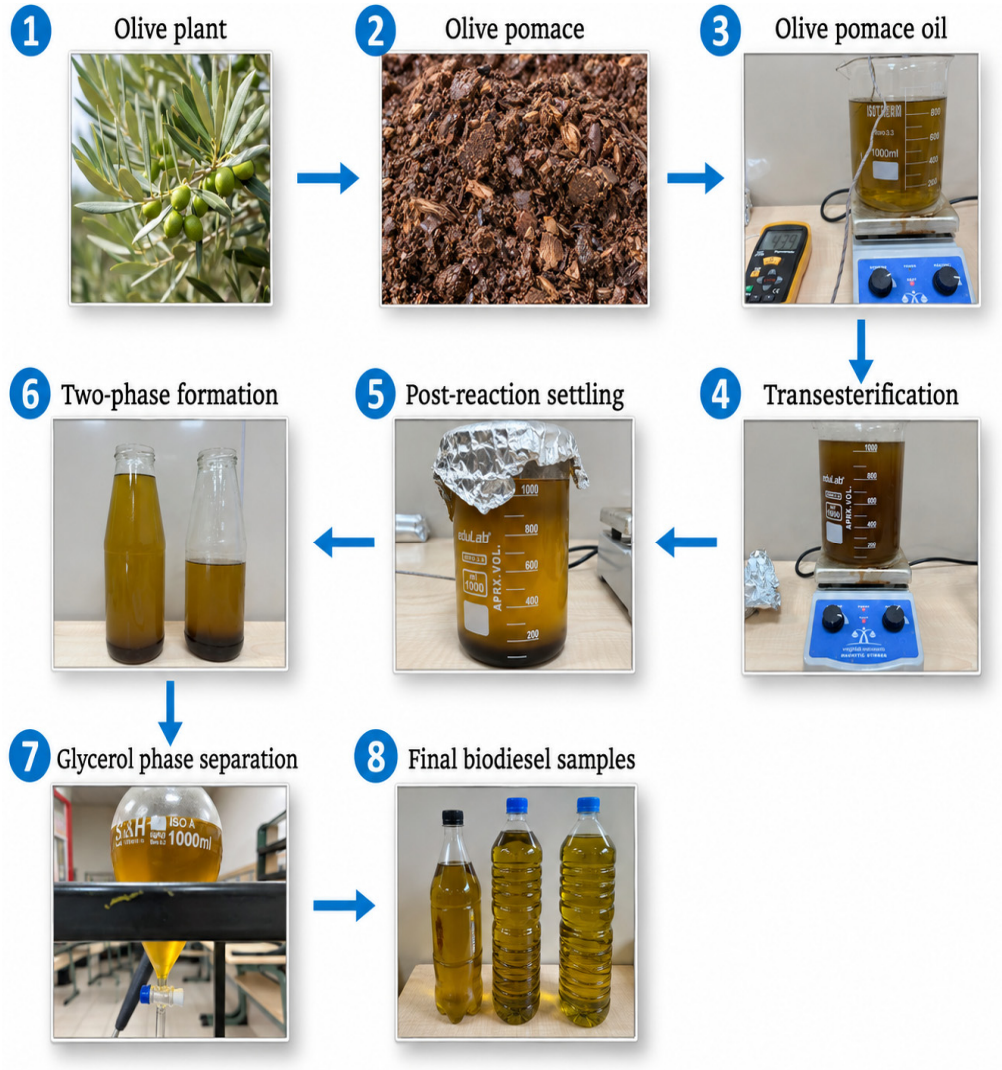

Figure 1. Production process of olive pomace oil biodiesel.

2.2. Preparation of Test Fuels

Table 1 lists the test fuel codes and compositions, while Table 2 summarizes the supplier specifications for the commercially sourced $BaCO_3$ and $BaTiO_3$ powders. Their reported nominal particle sizes were 780 nm (0.78 µm) and 90 nm, respectively. On the basis of these specifications and the conventional nanoscale range of approximately 1–100 nm [30], $BaCO_3$ is described as submicrometre particles and $BaTiO_3$ as nanoparticles. The available characterization does not establish a significant nanoscale fraction in the $BaCO_3$ powder. These values describe the supplied powders and do not represent hydrodynamic particle or agglomerate size distributions in BP50 [31]. Equal volumes of diesel and olive pomace oil methyl ester were combined to prepare the BP50 base fuel. Separate BP50 batches were formulated with either $BaCO_3$ or $BaTiO_3$ at nominal dosages of 25, 50, and 100 ppm. The nominal dosage labels of 25, 50, and 100 ppm correspond to particle additions of 0.025, 0.050, and 0.100 g per liter of BP50, respectively, equivalent to mass per volume loadings of 25, 50, and 100 mg L^{-1}. To aid dispersion after particle incorporation, each fuel underwent 30 min of sonication at 37 kHz in an Elmasonic S 60 H bath with a rated ultrasonic power of 150 W (Elma Schmidbauer GmbH, Singen, Germany). All test fuels were mixed immediately before engine testing. Each particle-containing formulation was magnetically stirred at 600 rpm for 10 min immediately before introduction into the engine to redistribute the suspended particles. The same procedure was applied to all six particle-containing

formulations to minimize preparation-related variability. The prepared suspensions were visually monitored over a 24 h observation period, during which no macroscopic phase separation was observed. No visible settling was detected during the visual inspections. These observations provided a qualitative assessment of macroscopic suspension behavior; particle size distributions and agglomeration within BP50 were not quantitatively characterized. Visual monitoring of sediment formation and phase separation has also been used as a qualitative assessment of suspension stability in recent nanoparticle-containing biodiesel studies [32–34]. Figure 2 illustrates the fuel preparation procedure.

Table 1. Fuel codes and compositions.

Fuel Code	Composition
D100	Pure diesel fuel
BP100	Pure olive pomace oil biodiesel
BP50	50% diesel + 50% olive pomace oil biodiesel
BP50BaCO25	BP50 + 25 ppm barium carbonate particles ($BaCO_3$)
BP50BaCO50	BP50 + 50 ppm barium carbonate particles ($BaCO_3$)
BP50BaCO100	BP50 + 100 ppm barium carbonate particles ($BaCO_3$)
BP50BaTiO25	BP50 + 25 ppm barium titanate particles ($BaTiO_3$)
BP50BaTiO50	BP50 + 50 ppm barium titanate particles ($BaTiO_3$)
BP50BaTiO100	BP50 + 100 ppm barium titanate particles ($BaTiO_3$)

Table 2. Properties of $BaCO_3$ and $BaTiO_3$ particles (values obtained from the supplier's technical specifications).

Property	Unit	$BaCO_3$	$BaTiO_3$
Chemical name	—	Barium carbonate	Barium titanate
Chemical formula	—	$BaCO_3$	$BaTiO_3$
Purity	%	99.98	99.95
Nominal particle size	nm	780	90
Density	g/cm^3	4.29	6.08



Figure 2. Preparation stages of the particle-added test fuels: (**a**) particles used in the study, (**b**) dispersion of the fuel particle mixtures in an ultrasonic bath, and (**c**) mixing of the prepared fuels using magnetic stirrers.

The micrographs in Figure 3 allow the dry $BaCO_3$ and $BaTiO_3$ powders to be compared at an identical magnification. $BaCO_3$ exhibits irregular and faceted particles whereas $BaTiO_3$ appears finer and more densely distributed, with partially rounded particles. Agglomerated clusters are visible in both samples. These images describe the morphology of the dry powders and do not establish the particle size distribution or dispersion stability within BP50.

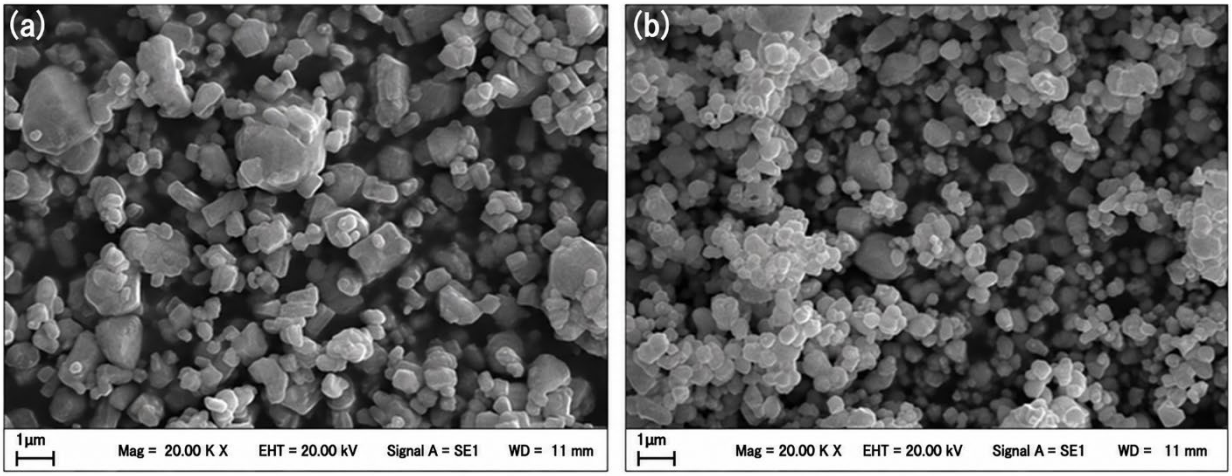

Figure 3. SEM images of the dry powders of (**a**) $BaCO_3$ and (**b**) $BaTiO_3$ before incorporation into BP50.

The supplier-reported characteristics of the $BaCO_3$ and $BaTiO_3$ powders are summarized in Table 2. The fuel properties of D100, BP50, and BP100 are summarized in Table 3. All properties presented in this table, including density at 15 °C, kinematic viscosity at 40 °C, flash point, cetane number, and lower heating value, were measured experimentally in the present study. The measured density, kinematic viscosity, and flash point values were broadly consistent with the corresponding property data reported in the literature for diesel, olive pomace oil methyl ester, and their blends [35–37]. These properties were considered when interpreting engine performance, exhaust emissions, smoke opacity, exhaust gas temperature and acoustic results.

Table 3. Fuel properties of D100, BP50 and BP100 fuels.

Fuel Code	Density at 15 °C, kg/m^3 (ASTM D4052)	Kinematic Viscosity at 40 °C, mm^2/s (ASTM D445)	Lower Heating Value, MJ/kg (ASTM D240)	Cetane Number (ASTM D613)	Flash Point, °C (ASTM D93)
D100	835	2.75	43.0	55.0	62
BP50	864	3.72	40.7	52.7	98
BP100	891	4.69	38.4	50.4	134

2.3. Engine Test Setup and Experimental Procedure

The test platform comprised a Cussons P8160 bench fitted with an Antor 6LD 400 diesel engine (Anadolu Motor, Çayırova-Kocaeli, Turkey) featuring one cylinder, a four stroke cycle, air cooling, and direct injection as shown in Figure 4. The technical specifications of the test engine are presented in Table 4. Brake loading was provided by a regenerative direct current dynamometer with an absorption capacity of 10 kW at 4000 rpm. Torque was obtained from a load cell incorporating strain gauges; rotational speed was monitored through a magnetic sensor operating with a toothed wheel. The original injection setting, a 28° crank angle before top dead center, was retained while a closed-loop controller regulated engine speed at 2000 rpm. The same protocol was applied to all fuels under ambient laboratory

conditions. After a 30 min warm-up, brake load was increased successively through 1, 1.5, 2, 2.5, and 3 kW. A 10 min operating interval with each newly introduced fuel allowed the preceding formulation to be cleared from the supply circuit. A separate stabilization period of 10 min was allowed after each load adjustment before measurements were recorded. For each fuel at each load, three measurements were collected, and the reported result represents their arithmetic average. The variability among these measurements was described by the sample standard deviation (SD). Fuel consumption was determined by using a stopwatch to measure the time required to consume a known volume from a graduated vessel.



Figure 4. Experimental setup and measurement devices used in the single-cylinder diesel engine tests.

A Bosch BEA 350 analyser was used to quantify HC, CO, CO_2, and NO_x in the exhaust. The Bosch RT430 smoke meter provided opacity measurements, which were recorded as percentages. The optical readings were retained as a measure of exhaust light attenuation, without conversion to particulate mass or particle number. The study did not quantify exhaust particulate mass, total particle number, or the distribution of particle sizes. Exhaust gas temperature was recorded using a CEM DT 610 instrument fitted with a K-type thermocouple probe. Sound pressure level was measured using a Benetech GM1352 sound level meter. Acoustic measurements were taken with the microphone positioned 1 m from the engine, approximately level with it. A-weighting was used for the sound measurements and the measured values are reported in dB(A). Before the engine was started, the background sound level in the laboratory was measured as 39.6 dB(A). Figure 5 shows the experimental workflow, beginning with the preparation of the test fuels and concluding with a comparative assessment of the results.

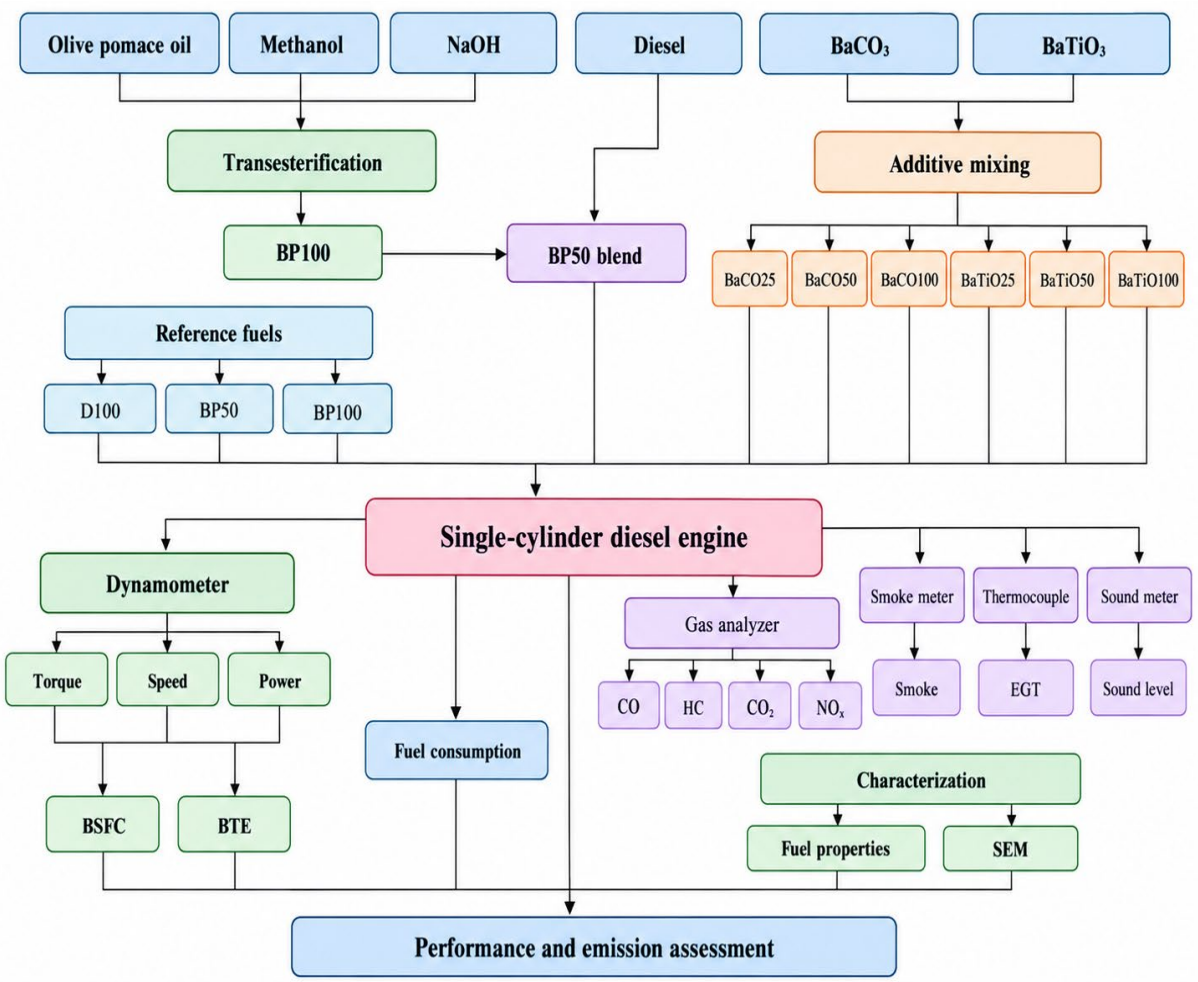

Figure 5. Experimental flowchart for the preparation, engine testing, and comparative evaluation of olive pomace oil biodiesel–diesel blends containing $BaCO_3$ or $BaTiO_3$ particles.

Table 4. Technical specifications of the test engine.

Parameter	Specification
Model	Antor 6LD 400
Engine cycle	Four-stroke
Number of cylinders	1
Bore/stroke	86/68 mm
Compression ratio	18:1
Maximum engine power	6.25 kW at 3600 min^{-1}
Fuel type	Diesel
Injection type	Direct injection
Injection pressure	200 kgf/cm^2
Injection timing	28° CA BTDC
Cooling type	Air cooled
Maximum engine speed	3600 min^{-1}

2.4. Performance Calculations and Uncertainty Analysis

Fuel consumption was determined using the volumetric measuring chamber incorporated into the engine test bench. At every operating condition, fuel consumption was timed over a predefined volume interval. Fuel density and the recorded consumption

interval were then used to calculate the mass flow associated with that volume, according to Equation (1):

$$\dot{m}_f = \frac{3600 \rho_f \Delta V_f}{10^6 \Delta t} \quad (1)$$

where $\dot{m}_f$ is the fuel mass flow rate (kg h^{-1}), ρ_f denotes the fuel density (kg m^{-3}), ΔV_f is the consumed fuel volume (mL), and Δt represents the corresponding measurement period (s). The factors 10^6 and 3600 account for the conversion of volume from milliliters to cubic meters and time from seconds to hours, respectively.

Brake specific fuel consumption (BSFC) relates the mass of fuel consumed to the brake output delivered. The volumetric consumption measurements were therefore expressed as a mass flow rate and normalized by measured brake power, giving BSFC in g kW^{-1} h^{-1} according to Equation (2):

$$\text{BSFC} = \frac{1000\, \dot{m}_f}{P_b} \quad (2)$$

where P_b denotes the measured brake power of the engine (kW). The multiplier of 1000 converts the fuel mass flow rate from kilograms per hour to grams per hour, allowing BSFC to be expressed in g kW^{-1} h^{-1}.

Brake thermal efficiency (BTE) was determined to assess the effectiveness of converting the chemical energy available in the consumed fuel into mechanical output at the engine shaft. The calculation incorporated the recorded shaft power, the associated fuel consumption rate on a mass basis, and the net calorific value of each investigated fuel formulation, as expressed below:

$$\text{BTE}\ (\%) = \frac{P_b \times 3600}{\dot{m}_f \times H_f} \times 100 \quad (3)$$

where P_b is the brake power (kW), $\dot{m}_f$ represents the fuel mass flow rate kg h^{-1}, and H_f denotes the lower heating value of the fuel (kJ kg^{-1}). The factor 3600 converts the hourly fuel consumption basis to seconds so that the energy input and brake power are expressed on a consistent time basis. Multiplication by 100 expresses the calculated efficiency as a percentage.

Instrumental uncertainty and experimental repeatability were reported separately. Table 5 summarizes the instrumental uncertainty estimates associated with the measurement devices. The sample standard deviations of the repeated measurements are not included in these estimates. For a derived quantity R that depends on independent input quantities x_i, the general root sum of squares relation for propagating standard uncertainties is given in Equation (4) [38].

$$u_c(R) = \sqrt{\sum_{i=1}^{n} \left(\frac{\partial R}{\partial x_i} \right)^2 u^2(x_i)} \quad (4)$$

Table 5. Relative uncertainty values used in the experimental assessment.

Parameter	Uncertainty (%)
CO	1.54
CO_2	1.48
HC	1.92
NO_x	1.03
BSFC	1.12
Smoke opacity	1.13
Thermocouple	0.66
Speed meter	0.92
Load cell	0.53
Noise meter	0.66

3. Results and Discussion

3.1. Brake Specific Fuel Consumption

The BSFC measurements obtained at a fixed speed of 2000 rpm are compared in Figure 6. Similar load-dependent behavior has been reported for biodiesel-fueled diesel engines [39,40]. D100 had the lowest BSFC at all loads. The BSFC of BP50 was 8.56–15.10% higher than that of D100, while BP100 showed an increase of 18.37–24.52%. The largest difference occurred at 3 kW where BP100 was 24.52% above D100. The biodiesel fuels provide less energy per unit mass than D100, while their greater density and viscosity can alter spray development. These property differences are compatible with the greater fuel mass required to deliver a given brake output [12,39]. Relative to additive-free BP50, the $BaCO_3$ containing formulations reduced BSFC by 2.29–3.80%, whereas the $BaTiO_3$-containing formulations produced reductions of 2.26–3.79%. Both additives gave their largest reduction at 2 kW and 50 ppm. Reductions in fuel consumption per unit of brake output following nanoparticle addition have also been documented in biodiesel studies [41,42].

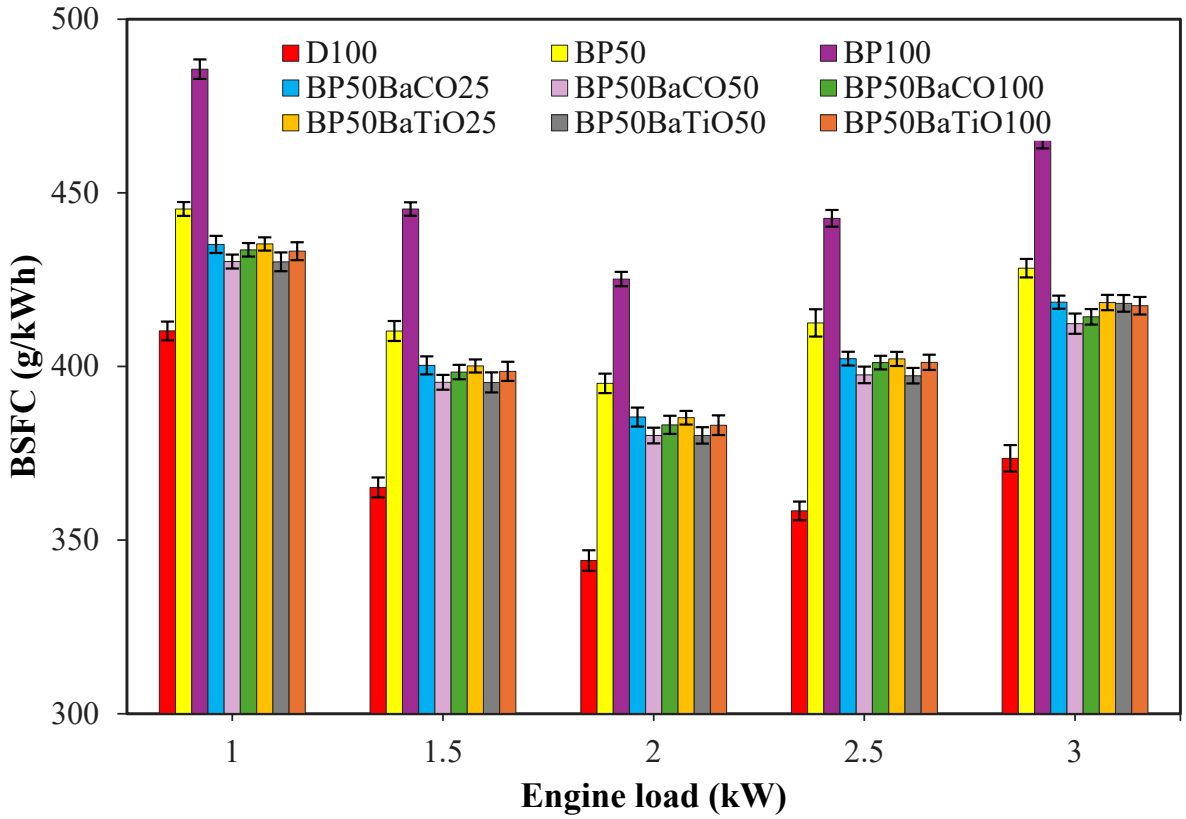

Figure 6. Effect of engine load on BSFC for the test fuels.

Increasing the concentration to 100 ppm did not provide a consistent additional benefit. Previous studies identify particle dispersion and suspension stability as constraints that depend on additive loading, providing a possible explanation for this response [43,44]. The 50 ppm formulations generally produced the lowest BSFC values within the investigated concentration range. In Figures 6–14, the columns represent the corresponding arithmetic means, and the error bars indicate ±1 SD ($n = 3$).

3.2. Brake Thermal Efficiency

In Figure 7, BTE increases between 1 and 2 kW, reaches its maximum at 2 kW, and then decreases as load approaches 3 kW. Earlier biodiesel engine experiments reported a comparable rise and subsequent fall in efficiency with increasing load [39,40]. D100 generally had

the highest BTE. Relative to D100, BTE was 2.69–8.22% lower with BP50 and 5.39–10.04% lower with BP100. The largest reduction occurred with BP100 at 3 kW. Changes in injection behavior and combustion characteristics may account for the BTE penalty observed with the biodiesel fuels. $BaCO_3$ and $BaTiO_3$ increased BP50 BTE by 2.32 to 3.98% depending on load and concentration. At 2 kW, both 50 ppm formulations increased BTE from approximately 22.38% to 23.27%, corresponding to a relative improvement of 3.98%.

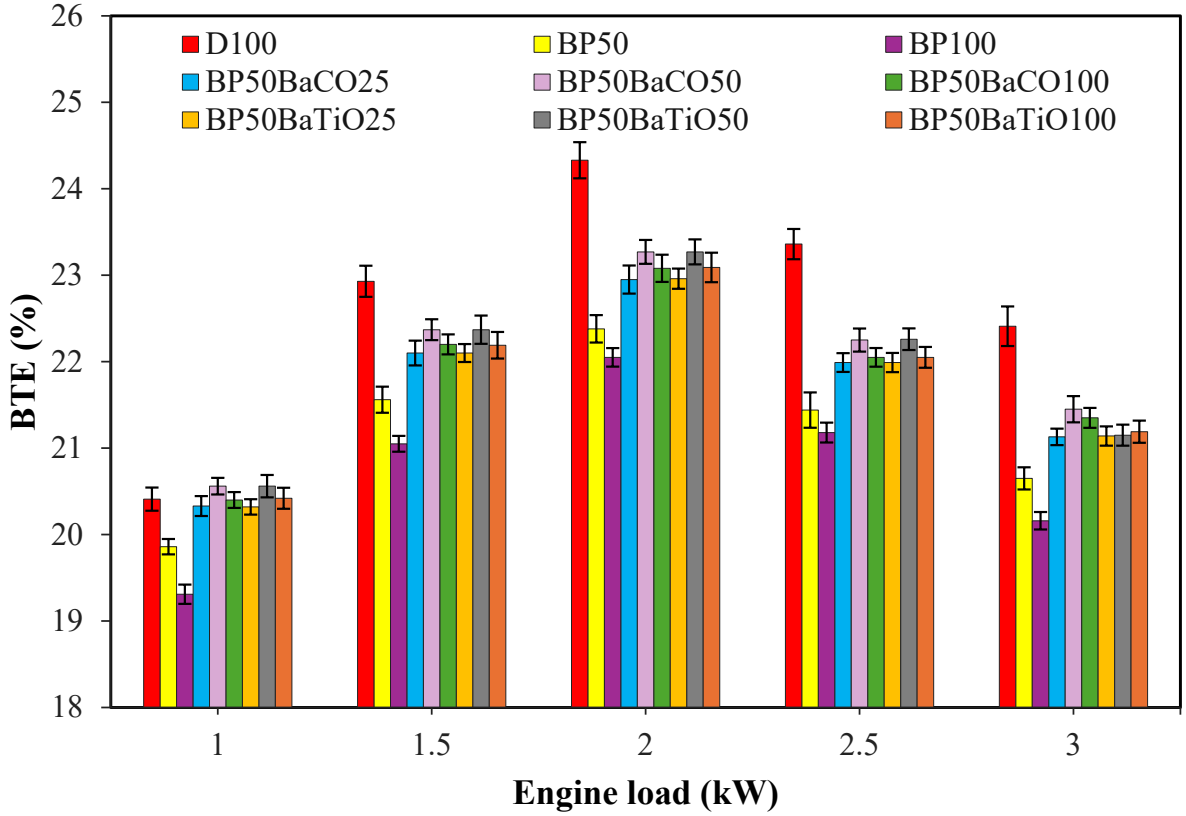

Figure 7. Effect of engine load on BTE for the test fuels.

Comparable improvements in BTE have been reported for nanoparticle-containing biodiesel and diesel blends [41,45]. At 1 kW the 50 ppm $BaCO_3$ and $BaTiO_3$ blends were approximately 0.73% above D100 but D100 remained higher at the other loads. No consistent further gain in BTE was observed at a particle loading of 100 ppm. Concentration-dependent changes in particle dispersion and suspension stability provide a plausible explanation for such nonlinearity [43,44], although stability was not quantified in the present work. At 3 kW the 50 ppm $BaCO_3$ blend had a BTE approximately 1.42% higher than the corresponding $BaTiO_3$ blend. A loading of 50 ppm was generally favorable for BTE, the relative performance of the $BaTiO_3$ formulations nevertheless depended on the imposed load. Channapattana et al. [46] investigated NiO nanoparticles in a blend containing 25% neem methyl ester using cylinder pressure, heat release, energy and exergy analyses at different static injection timings. In that experiment, advancing injection from 23° to 27° before top dead center altered the energy balance. These findings illustrate why efficiency changes in particle-containing fuels should be interpreted together with combustion conditions rather than attributed solely to fuel heating value.

3.3. Sound Level Characteristics

Figure 8 shows that sound level increased progressively as the applied engine load increased across the investigated fuel formulations. From 1 to 3 kW, the measured sound

level increased by 3.9 to 4.1 dB(A), depending on fuel type. Fuel-dependent changes in diesel engine noise have also been reported in experimental studies using biodiesel and nanoparticle fuels [19,47].

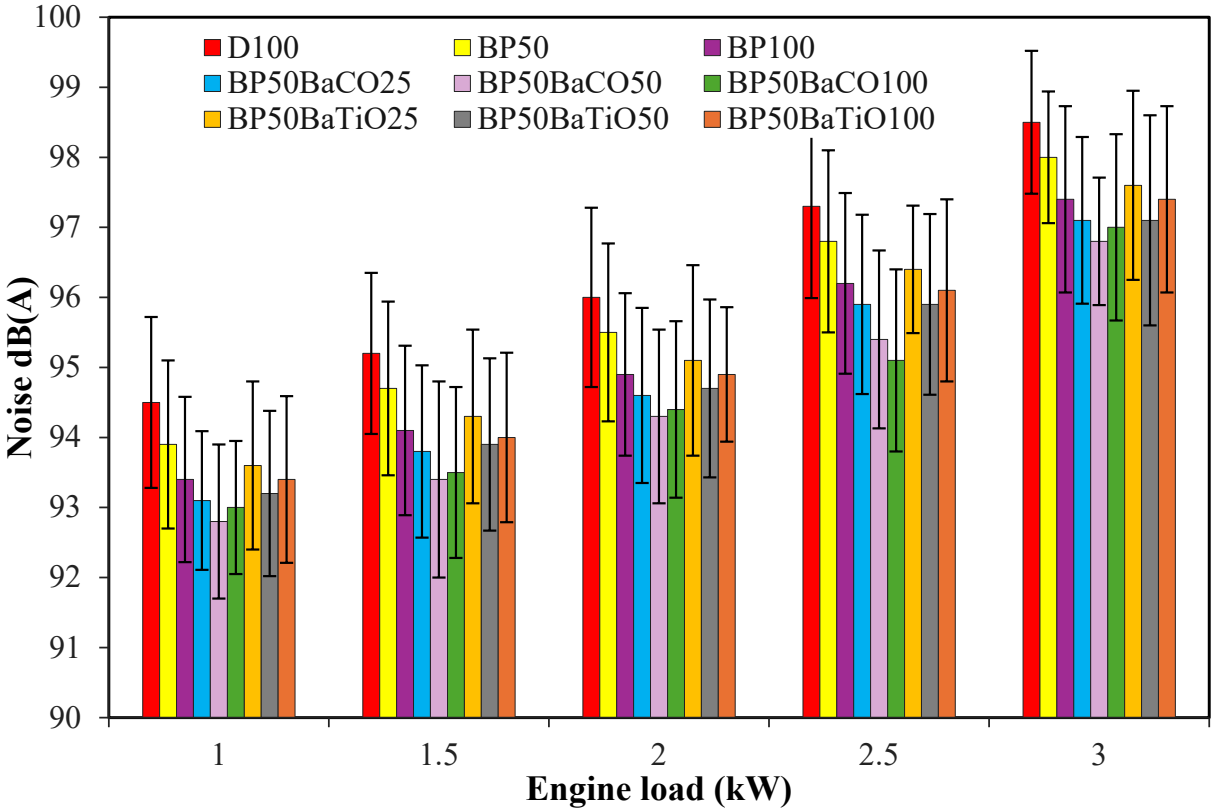

Figure 8. Effect of engine load on sound level for the test fuels.

D100 produced the highest measured sound level at every load. BP50 was 0.5 to 0.6 dB(A) lower than D100 and BP100 was 1.1 dB(A) lower. Because the measured sound pressure level includes both combustion and mechanical contributions, the observed differences should not be attributed to cetane number or ignition delay alone. Relative to BP50 the $BaCO_3$ blends were 0.8 to 1.7 dB(A) lower while the $BaTiO_3$ blends were 0.3 to 0.9 dB(A) lower. The largest $BaCO_3$ difference was 1.7 dB(A) at 100 ppm and 2.5 kW. The 50 ppm $BaCO_3$ blend gave a consistent reduction of 1.1 to 1.4 dB(A) across the load range. The 50 ppm $BaTiO_3$ blend was 0.7 to 0.9 dB(A) lower than BP50. At a given particle loading, sound levels from the $BaCO_3$ formulations were 0.3–1.0 dB(A) below those from the corresponding $BaTiO_3$ formulations. Several differences between fuels were comparable in magnitude to the associated standard deviations. In the absence of inferential testing, these acoustic results are therefore treated as descriptive comparisons. Within the present test setup, $BaCO_3$ formulations generally produced numerically lower A-weighted sound pressure levels than the corresponding $BaTiO_3$ formulations.

3.4. HC Emissions

Figure 9 shows that HC emissions declined with increasing engine load up to 2.5 kW and then increased at 3 kW. The decrease in HC at intermediate loads may reflect more favorable oxidation conditions, whereas the increase at 3 kW may be associated with greater mixture inhomogeneity and locally fuel-rich regions. BP50 reduced HC by 5.56 to 9.09% relative to D100 and BP100 reduced it by 9.09 to 16.67%. The maximum BP100 reduction occurred at 2 kW. The oxygen content of biodiesel can support oxidation of unburned fuel,

although higher viscosity can adversely affect atomization [13,48]. $BaCO_3$ reduced HC from BP50 by 16.67 to 40.00%. The largest reduction was 40.00% at 2.5 kW with 100 ppm. The same concentration reduced HC by 33.33% at 1.5 kW and 36.36% at 2 kW. $BaTiO_3$ produced reductions of up to 30.00% and its largest reduction occurred at 2.5 kW with 50 ppm. At 50 ppm the reductions were 17.65%, 20.00%, 18.18%, 30.00% and 25.00% at 1, 1.5, 2, 2.5 and 3 kW respectively. Previous studies have reported similar reductions in HC for biodiesel blends and ternary fuels containing nanoparticles [49,50]. More recently, Torkzaban et al. [51] investigated pomegranate peel-derived carbon quantum dots at 100–600 ppm in a B20 blend prepared from waste frying oil biodiesel.

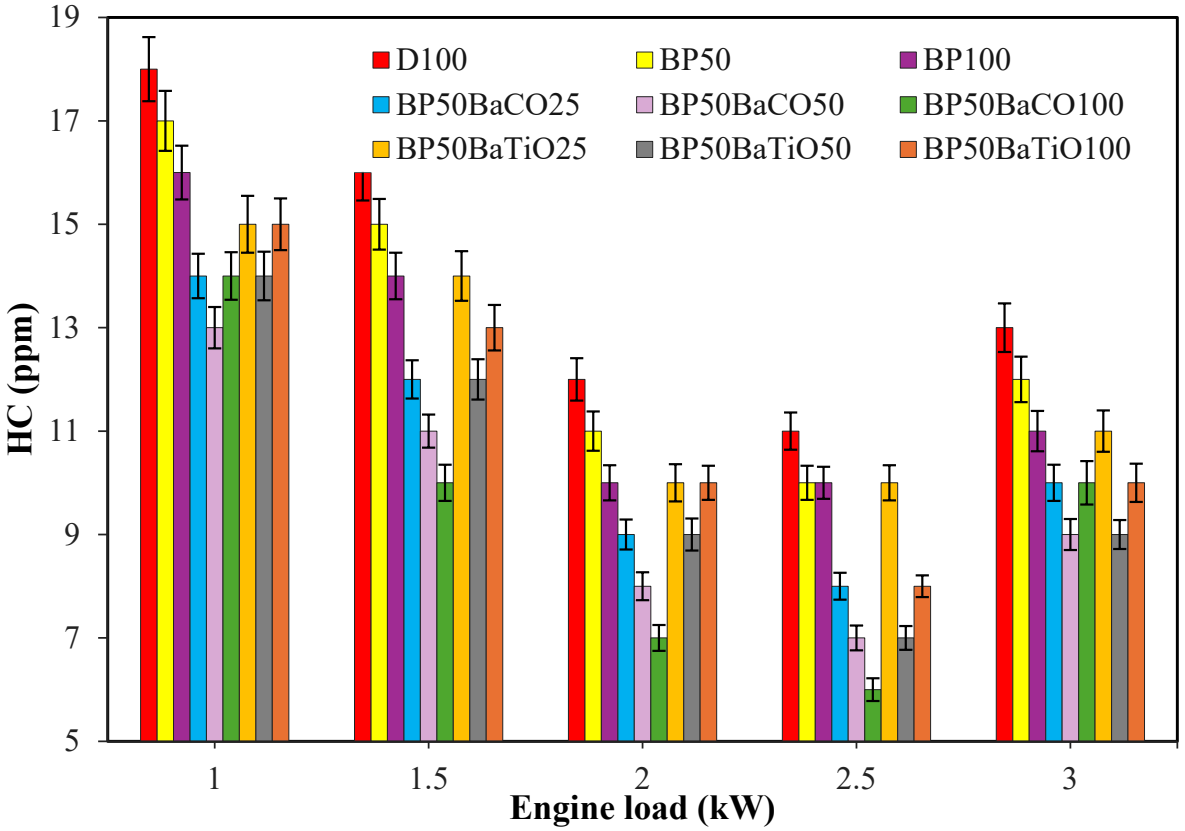

Figure 9. Effect of engine load on HC emissions for the test fuels.

The selected 600 ppm formulation produced lower CO and unburned hydrocarbon emissions than neat diesel. This extends the reported incomplete combustion benefits to a carbon-based additive, although its reference fuel and concentration range differ from the BP50-based comparisons used here. The concentration response was not linear. Within the $BaCO_3$ series, the lowest HC concentrations were obtained with 100 ppm at 1.5–2.5 kW and with 50 ppm at 1 and 3 kW. Within the $BaTiO_3$ series, the 50 ppm formulation produced the lowest HC concentrations across the investigated loads. Previous studies have also reported that the effects of particulate additives can vary with concentration, particle characteristics and preparation conditions [43,44]. At equal concentrations, $BaCO_3$ generally produced lower HC than $BaTiO_3$, especially at 100 ppm under medium loads.

3.5. CO Emissions

Figure 10 shows that CO increased with engine load and rose more sharply above 2 kW. Greater fuel delivery at high load can promote locally fuel-rich regions, which may limit complete CO oxidation. BP50 reduced CO by 10.53 to 16.19% relative to D100 and BP100 reduced it by 25.93 to 36.19%. The largest reductions for both fuels were observed at

2.5 kW. These reductions are consistent with the oxygenated nature of biodiesel, although fuel viscosity and spray characteristics may also influence CO formation [13,52].

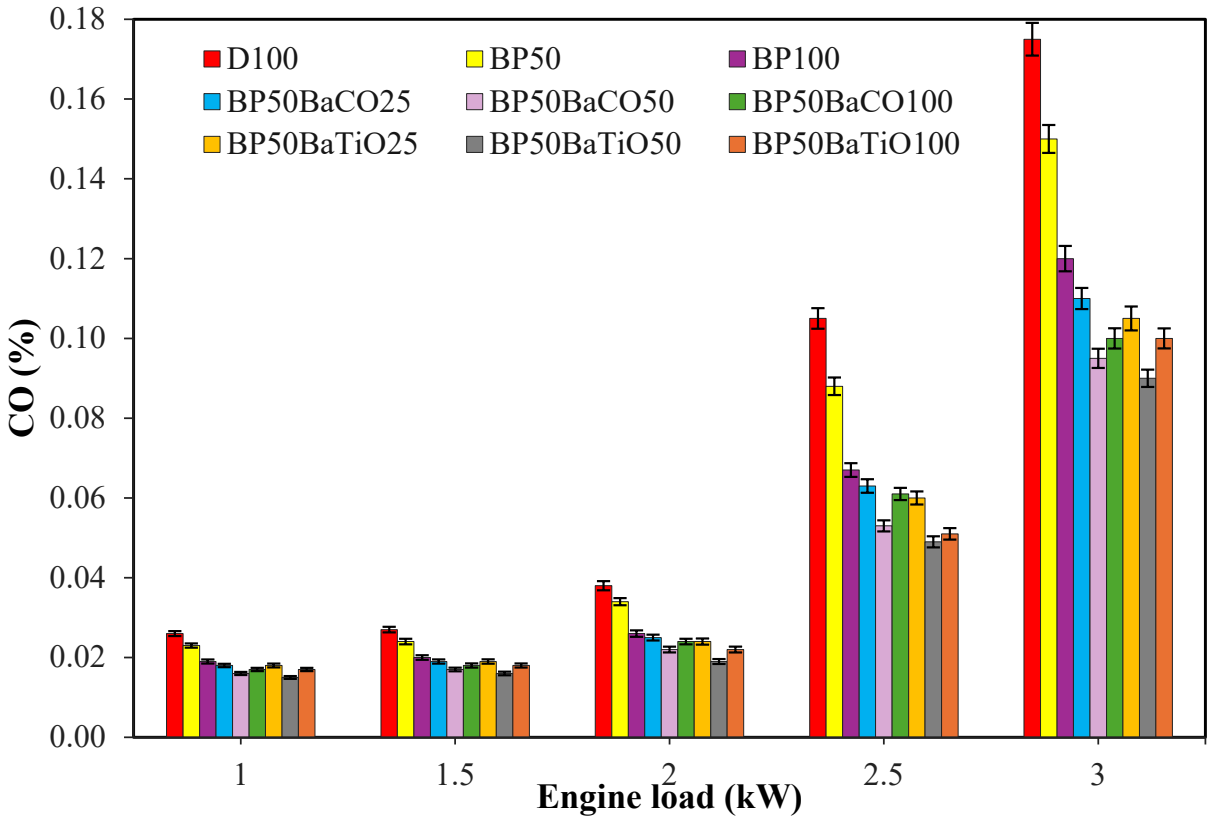

Figure 10. Effect of engine load on CO emissions for the test fuels.

Both additives further reduced CO concentrations relative to additive-free BP50. $BaCO_3$ reduced CO by 20.83 to 39.77% and $BaTiO_3$ by 20.83 to 44.32%. The largest reductions occurred at 2.5 kW and 50 ppm where $BaCO_3$ and $BaTiO_3$ reduced CO by 39.77% and 44.32% respectively. Gamboa et al. [53] evaluated functionalized and non-functionalized carbon nanotubes in commercial diesel and palm oil biodiesel. In the biodiesel formulations, nanotube addition increased thermal efficiency and reduced CO emissions, while amide functionalization improved the dispersion of nanotubes in commercial diesel. Their findings show that the base fuel and particle surface treatment are relevant to the observed response.

3.6. CO_2 Emissions

Figure 11 shows that the exhaust CO_2 concentration increased with engine load for all fuel formulations. D100 had the lowest values. Relative to D100 BP50 increased CO_2 by 4.30 to 7.62% and BP100 increased it by 12.39 to 17.07%. The largest absolute difference for BP100 occurred at 3 kW. The higher exhaust CO_2 concentrations, together with lower CO concentrations, are compatible with a shift toward more complete carbon oxidation. However, concentration measurements alone do not establish changes in the CO_2 mass emission rate because exhaust flow was not quantified. Adding $BaCO_3$ to BP50 increased CO_2 by 1.87 to 7.46% while $BaTiO_3$ produced increases of 1.35 to 6.23%. The largest increases occurred at 1 kW for 100 ppm $BaCO_3$ and at 1.5 kW for 100 ppm $BaTiO_3$. A simultaneous increase in CO_2 with reductions in CO and HC has been reported for TiO_2 enhanced biodiesel blends, consistent with more complete oxidation under some operating conditions [54].

The response was not linear with concentration and the differences between $BaCO_3$ and $BaTiO_3$ remained small at 25 and 50 ppm. The increase in engine out CO_2 should not be

interpreted as a direct measure of the lifecycle greenhouse gas impact of biodiesel because the carbon originates partly from renewable biomass [5].

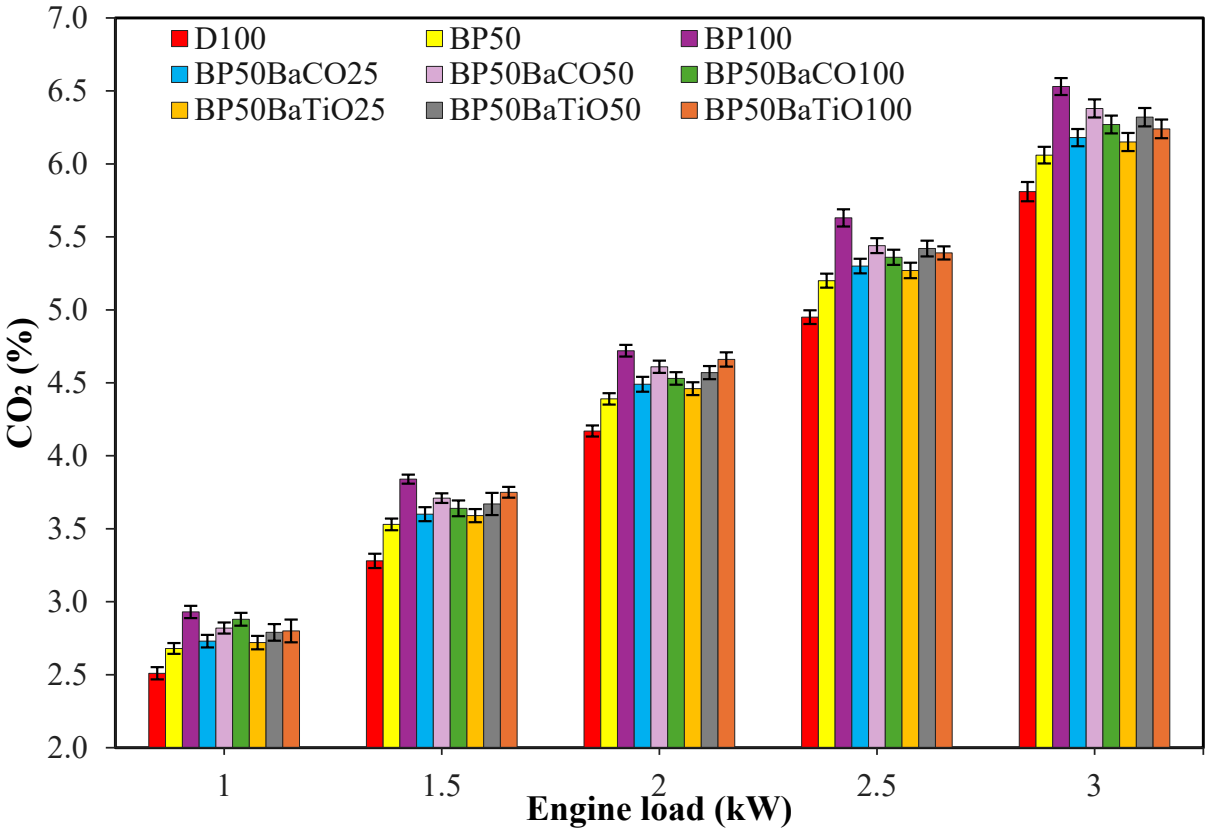

Figure 11. Effect of engine load on CO_2 emissions for the test fuels.

3.7. NO_X Emissions

Figure 12 shows that NO_X emissions increased with engine load for all fuels. D100 produced the lowest NO_X at all loads. BP50 was 12.50 to 22.96% higher than D100 and BP100 was 23.13 to 42.86% higher. The largest difference occurred with BP100 at 3 kW. Higher NO_X with olive pomace biodiesel has also been reported in direct OPME engine studies [13,14]. The present trend may be consistent with the combined effect of oxygen availability and higher local combustion temperature. The EGT results provide complementary information on the exhaust's thermal state but do not establish changes in peak in-cylinder temperature or high-temperature residence time.

$BaCO_3$ and $BaTiO_3$ further increased NO_X from BP50. The $BaCO_3$ increase ranged from 0.56 to 10.58% while the $BaTiO_3$ increase ranged from 2.90 to 19.87%. For both additives, the largest increase occurred at 2 kW and 100 ppm. Under these conditions, NO_x increased by 10.58% with $BaCO_3$ and 19.87% with $BaTiO_3$. The increase in NO_X following particle addition should be considered together with the accompanying reductions in CO, HC and smoke opacity, as well as the improvement in BTE relative to BP50. These combined responses may reflect changes in oxidation during combustion. A possible catalytic contribution is the acceleration of reactions at particle surfaces, which could modify the location and timing of heat release. If oxidation were enhanced in hot regions early in the combustion process, local temperature and oxygen radical availability could increase, favoring thermal NO_X formation [55,56]. Such effects would not require a uniform temperature increase throughout the cylinder. Conversely, a shorter ignition delay could reduce the fuel accumulated before combustion and moderate the initial premixed heat release. For $BaCO_3$, a possible contribution to oxidation must be distinguished from direct oxygen

release. Hong et al. [57] demonstrated that $BaCO_3$ nanoparticles enhanced oxygen surface exchange and accelerated surface reaction kinetics on mixed-oxide electrodes. Although those electrochemical conditions differ from diesel combustion, the findings provide a mechanistic basis for considering a contribution from interfacial oxygen reactions. Such a contribution could facilitate the use of oxygen already present in the reacting mixture rather than supply additional molecular oxygen. The thermal decomposition of $BaCO_3$, expressed as $BaCO_3 \rightarrow BaO + CO_2$, is endothermic and produces CO_2 rather than O_2 [58]. Consequently, the NO_X increase with $BaCO_3$ is more appropriately discussed in terms of its possible influence on fuel oxidation and the resulting local thermal conditions, not as a consequence of assumed O_2 release from the carbonate. The measured EGT and NO_x responses did not follow the same ranking. $BaCO_3$ generally produced slightly higher EGT than $BaTiO_3$ at matched concentrations, despite lower NO_X concentrations. Furthermore, the highest EGT generally occurred at 50 ppm, whereas NO_X continued to increase as the additive concentration rose to 100 ppm. These observations show that EGT cannot be used as a surrogate for the local thermal conditions governing NO formation. EGT characterizes the exhaust after expansion and heat transfer, whereas thermal NO formation depends on local temperature, oxygen availability and residence time in hot reacting regions [55,56]. In the present study NO_X increased progressively with concentration and $BaTiO_3$ consistently produced higher NO_X than $BaCO_3$ at equal concentrations. Depending on load the $BaTiO_3$ values were 0.94 to 3.78% higher at 25 ppm, 2.69 to 7.41% higher at 50 ppm and 6.81 to 9.74% higher at 100 ppm than the corresponding $BaCO_3$ fuels. At 50 ppm, neither additive improved all measured outcomes simultaneously. Despite lower BSFC, CO concentrations, and smoke opacity, together with higher BTE, NO_X concentrations increased by 2.79–3.53% with $BaCO_3$ and 6.11–10.41% with $BaTiO_3$ relative to BP50. The nitrogen oxide increase was therefore more pronounced for $BaTiO_3$.

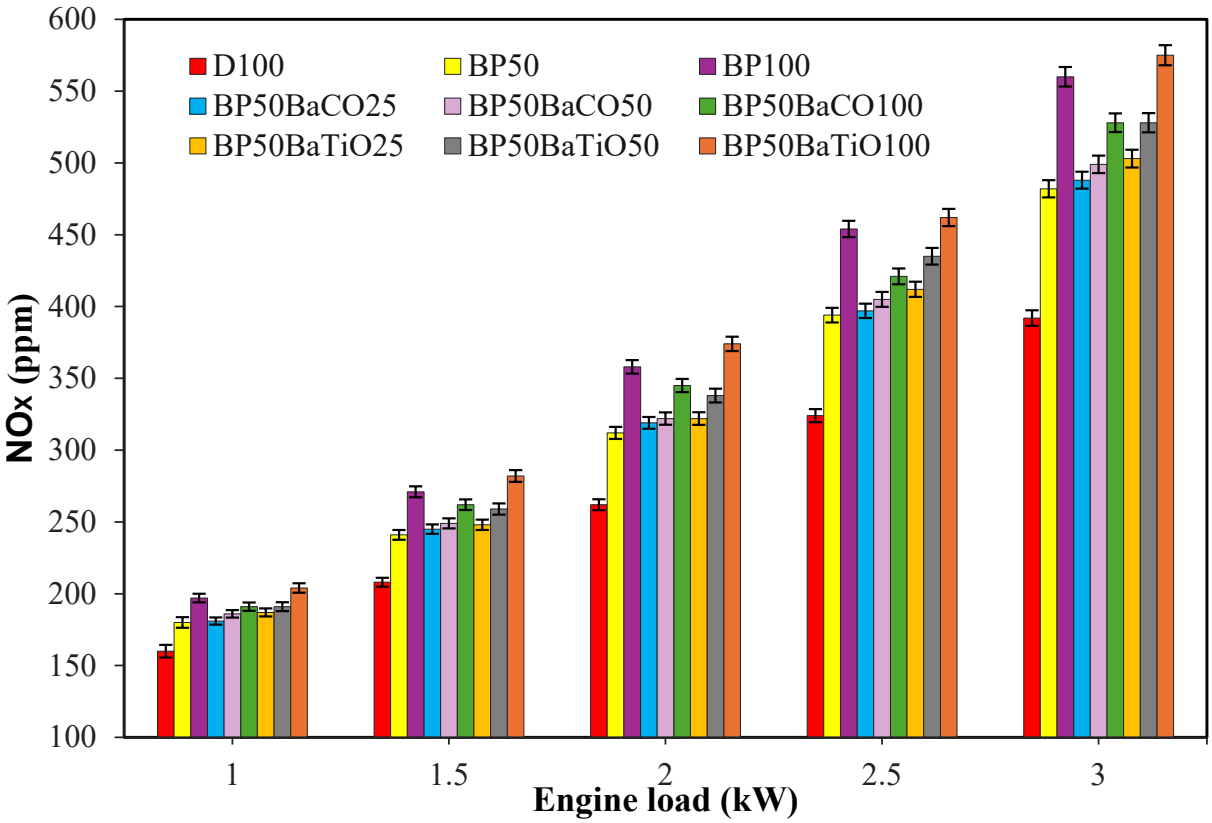

Figure 12. Effect of engine load on NO_X emissions for the test fuels.

3.8. Smoke Opacity

Figure 13 indicates a progressive increase in exhaust smoke opacity as engine loading intensified, with a pronounced increase observed at the maximum load of 3 kW. Relative to D100, the measured opacity was 1.19–40.74% lower with BP50. BP100 also produced lower opacity at most loads, with a maximum relative reduction of 56.67% at 2 kW. However, its opacity was 7.14% higher than that of D100 at 2.5 kW. This load response may reflect differences in fuel mixing and oxidation conditions associated with fuel oxygen content and viscosity [13,48]. Relative to BP50, $BaCO_3$ formulations reduced measured smoke opacity by 13.26–31.25%, while $BaTiO_3$ formulations produced reductions of 11.47–26.92%. The lowest opacity values were generally observed at 50 ppm. The maximum relative reductions were 31.25% for $BaCO_3$ at 1 kW and 26.92% for $BaTiO_3$ at 1.5 kW. At 3 kW, the 50 ppm $BaCO_3$ and $BaTiO_3$ formulations reduced opacity by 23.30% and 20.07%, respectively. Increasing the concentration from 50 to 100 ppm did not consistently lower opacity further. At equal concentrations, $BaCO_3$ generally produced lower measured opacity than $BaTiO_3$. Comparable reductions in smoke opacity have been reported for other biodiesel formulations containing metal oxide additives [49,59].

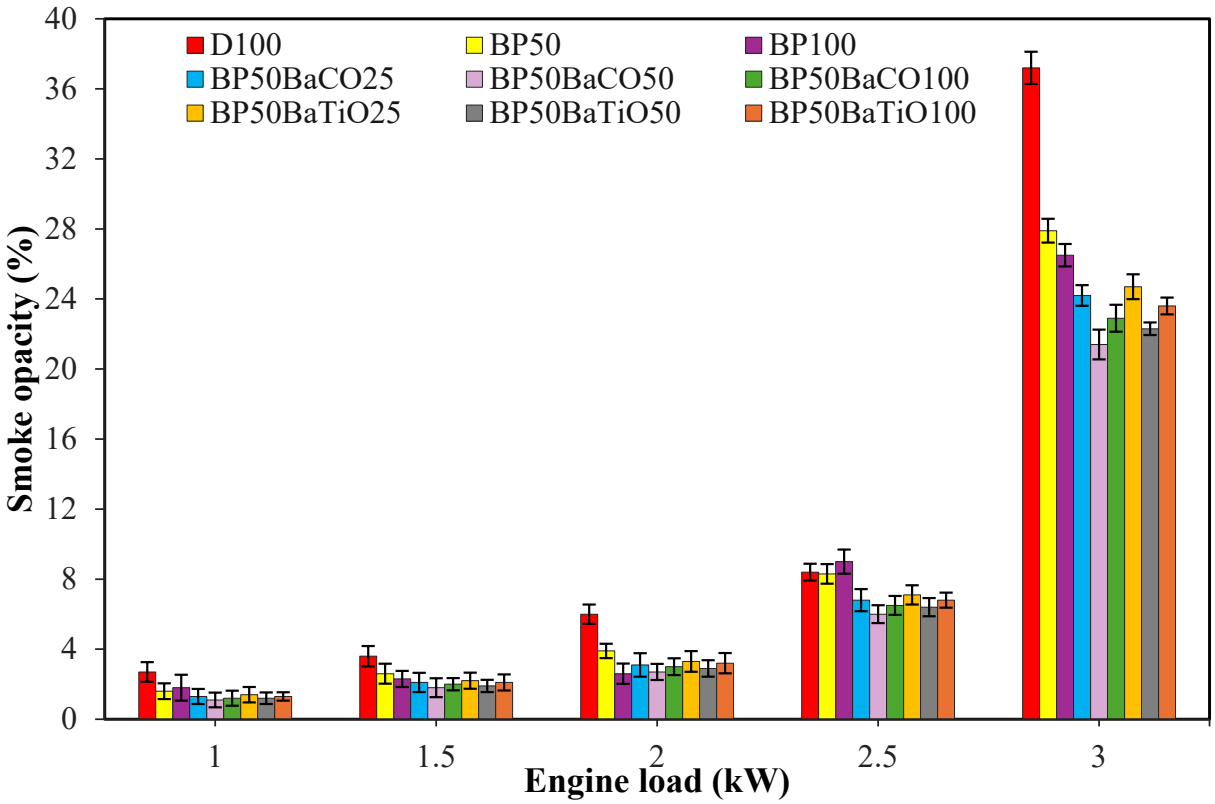

Figure 13. Effect of engine load on smoke opacity for the test fuels.

These optical comparisons should be distinguished from measurements of soot concentration and particle number. Guo et al. [60] reported higher soot concentrations for diesel containing nano Al_2O_3 under their spray combustion conditions. Jain et al. [61] demonstrated that total particle number and the number within specific size intervals can respond differently during the flame combustion of diesel containing TiO_2. For their 100 ppm formulation prepared by ball milling and bath sonication, the total number concentration over 15.7–637.8 nm decreased by 37.70%, whereas the concentration in the 23–50 nm interval increased by 16.73%. These results support the need for measurements across particle size intervals. Gallego et al. [62] also examined fuel filter retention and particulate emissions

for diesel containing carbon nanotubes, addressing aspects that cannot be assessed from smoke opacity alone.

3.9. Exhaust Gas Temperature Characteristics

Figure 14 shows that exhaust gas temperature increased continuously with engine load. Increasing the load from 1 to 3 kW raised EGT by 167–191 °C, depending on the fuel. D100 had the lowest EGT at every load. EGT was 14–23 °C higher for BP50 and 24–48 °C higher for BP100 than for D100.

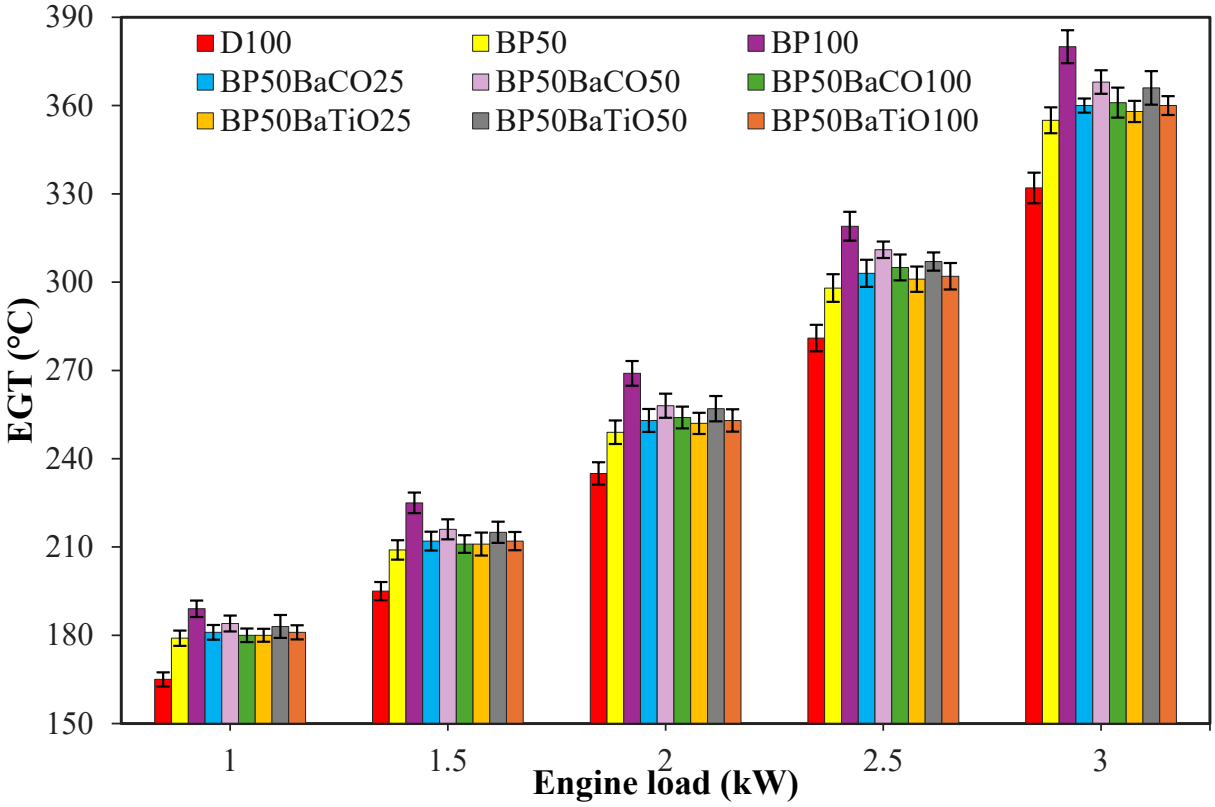

Figure 14. Effect of engine load on EGT for the test fuels.

The largest EGT difference between BP100 and D100 occurred at 3 kW. The lower heating value and higher density and viscosity of biodiesel can increase the required fuel quantity and alter the timing of heat release which can raise exhaust temperature [39,40]. Relative to BP50, $BaCO_3$ increased EGT by 1–13 °C and $BaTiO_3$ by 1–11 °C across the tested conditions. The largest absolute EGT increases were 13 °C for 50 ppm $BaCO_3$ at 2.5 and 3 kW and 11 °C for 50 ppm $BaTiO_3$ at 3 kW. The present increase in EGT is not a universal response to particle addition. Özer et al. [63] reported increased EGT, NO_X and CO_2 together with lower HC, CO, BSFC and smoke opacity when investigating borax decahydrate containing diesel methanol fuels. This combination resembles several responses observed here and shows that lower CO and HC concentrations and lower smoke opacity can coexist with higher exhaust gas temperatures and nitrogen oxide concentrations. This pattern contrasts with the lower EGT reported by Ağbulut and Sarıdemir [64] and in other nanoparticle fuel studies [54,65], indicating that the response depends on fuel formulation and operating conditions.

Both additives produced their highest EGT at 50 ppm in the present study. Increasing the concentration to 100 ppm did not produce a consistent additional increase. Concentration-dependent dispersion and stability effects provide a plausible explana-

tion [43,44], although suspension stability was not quantified here. $BaCO_3$ generally produced slightly higher EGT than $BaTiO_3$ at equal concentrations. The largest difference between the two additives at an equal concentration was 4 °C, observed at 2.5 kW and 50 ppm. Higher EGT alone does not establish improved efficiency or quantify exhaust energy loss, which also depends on exhaust mass flow and thermophysical properties.

4. Conclusions

This study compared $BaCO_3$ and $BaTiO_3$ particles in a 50:50 olive pomace oil biodiesel–diesel blend at 2000 rpm and loads of 1–3 kW. Increasing the biodiesel fraction generally reduced CO and HC concentrations and smoke opacity, increased BSFC and EGT, raised CO_2 and NO_X concentrations, and reduced BTE. Relative to D100, BP100 increased BSFC and NO_X by up to 24.52% and 42.86%, respectively. Both additives reduced BSFC and increased BTE relative to BP50. At 2 kW, the 50 ppm $BaCO_3$ and $BaTiO_3$ blends reduced BSFC by 3.80% and 3.79%, respectively, while BTE increased from approximately 22.38% to 23.27%. The emission response depended on both the additive and engine load. The largest reductions relative to BP50 were 44.32% for CO with 50 ppm $BaTiO_3$ at 2.5 kW, 40.00% for HC with 100 ppm $BaCO_3$ at 2.5 kW, and 31.25% for smoke opacity with 50 ppm $BaCO_3$ at 1 kW. Both additives increased NO_x, with the largest increase reaching 19.87% for 100 ppm $BaTiO_3$ at 2 kW. At 50 ppm, the NO_x increase was 2.79–3.53% for $BaCO_3$ and 6.11–10.41% for $BaTiO_3$ across the tested loads. Increasing the additive concentration from 50 to 100 ppm did not consistently improve thermal efficiency or further reduce fuel consumption, carbon monoxide and hydrocarbon concentrations, or smoke opacity. Compared with the unmodified blend, the formulation containing 50 ppm of $BaCO_3$ reduced fuel consumption, smoke opacity and sound pressure level, while its nitrogen oxide increase was smaller than that of the corresponding $BaTiO_3$ formulation. These comparisons are restricted to the measured responses and do not establish a reduction in particulate pollution or a universal optimum beyond the investigated conditions. Further work should investigate combustion behavior using crank-angle-resolved in-cylinder pressure measurements and the corresponding apparent heat release analysis, alongside assessments of long-term dispersion stability, fuel filter retention, emitted particulate composition, engine durability and strategies to limit the associated nitrogen oxide increase.

Cold flow properties were not evaluated in the present study. Future work should determine the cloud point, pour point, and cold filter plugging point of D100, BP50, BP100, and the BP50 formulations containing $BaCO_3$ or $BaTiO_3$, using standardized methods appropriate for the fuel samples. Controlled cooling and repeated cooling–warming cycles should also be used to evaluate changes in viscosity, particle agglomeration and sedimentation, and filterability. Complementary cold start tests at defined ambient temperatures would help establish the low-temperature operating limits of these fuels and determine whether the benefits observed under the present test conditions are retained during cold-weather operation.

Author Contributions: Conceptualization, İ.G., F.O. and T.G.; methodology, İ.G. and F.O.; investigation, İ.G.; formal analysis, İ.G.; writing—original draft preparation, İ.G.; writing—review and editing, İ.G., F.O. and T.G.; supervision, T.G. All authors have read and agreed to the published version of the manuscript.

Funding: This research was supported by the Scientific Research Projects Unit of Fırat University (FUBAP), project numbers TEKF.24.40 and TEKF.26.58.

Institutional Review Board Statement: Not applicable.

Informed Consent Statement: Not applicable.

Data Availability Statement: The experimental data and characterization results generated and analyzed during this study are available from the corresponding author upon reasonable request.

Acknowledgments: This study is derived from a part of the Ph.D. thesis of the first author (İbrahim Gündüz). The authors would like to thank the Scientific Research Projects Unit of Firat University (FUBAP) for supporting this study through project TEKF. 24.40 and TEKF. 26.58. The authors also acknowledge the support provided for the open access publication process of this study. During the preparation of this manuscript, OpenAI's ChatGPT (San Francisco, CA, USA, GPT-5.5, 2026 release) was used to improve the readability of selected sections and correct language errors. All generated content was carefully reviewed and edited by the authors, and the authors take full responsibility for the final published version of the manuscript.

Conflicts of Interest: The authors declare no conflicts of interest.

Nomenclature

$BaCO_3$	Barium carbonate
$BaTiO_3$	Barium titanate
D100	100% petroleum diesel fuel
BP100	Pure olive pomace oil biodiesel
BP50	50% diesel + 50% olive pomace oil biodiesel
BP50BaCO25	BP50 + 25 ppm $BaCO_3$
BP50BaCO50	BP50 + 50 ppm $BaCO_3$
BP50BaCO100	BP50 + 100 ppm $BaCO_3$
BP50BaTiO25	BP50 + 25 ppm $BaTiO_3$
BP50BaTiO50	BP50 + 50 ppm $BaTiO_3$
BP50BaTiO100	BP50 + 100 ppm $BaTiO_3$
HC	Hydrocarbon
CO_2	Carbon dioxide
CO	Carbon monoxide
NO_X	Nitrogen oxides
BTE	Brake thermal efficiency (%)
BSFC	Brake specific fuel consumption (g/kWh)
EGT	Exhaust gas temperature (°C)
LHV	Lower heating value (MJ/kg)
CI	Compression ignition
rpm	Revolutions per minute
ppm	Parts per million

References

1. Mahmudul, H.M.; Hagos, F.Y.; Mamat, R.; Adam, A.A.; Ishak, W.F.W.; Alenezi, R. Production, Characterization and Performance of Biodiesel as an Alternative Fuel in Diesel Engines—A Review. *Renew. Sustain. Energy Rev.* **2017**, *72*, 497–509. [CrossRef]
2. Mulk, W.U.; Ismael, M.A.; Aziz, A.R.A.; Azman, M.; Aider, M.; Younas, M.; Hamdy, M.; Nemitallah, M.A. Recent Progress in Biodiesel-Fueled ICEs and Role of Nano-Additives in Optimizing Combustion and Emissions with Cost Analysis—A Comprehensive Review. *Renew. Sustain. Energy Rev.* **2026**, *226*, 116263. [CrossRef]
3. Hosseini, S.H.; Taghizadeh-Alisaraei, A.; Ghobadian, B.; Abbaszadeh-Mayvan, A. Effect of Added Alumina as Nano-Catalyst to Diesel-Biodiesel Blends on Performance and Emission Characteristics of CI Engine. *Energy* **2017**, *124*, 543–552. [CrossRef]
4. Hazar, H.; Oflaz, F.; Sevinc, H. Effects of Pomegranate Seed Oil Methyl Ester Concentration and Fuel Preheating on Diesel Engine Performance, Emissions, and Operating Characteristics. *J. Therm. Anal. Calorim.* **2026**. [CrossRef]
5. Rajaeifar, M.A.; Akram, A.; Ghobadian, B.; Rafiee, S.; Heijungs, R.; Tabatabaei, M. Environmental Impact Assessment of Olive Pomace Oil Biodiesel Production and Consumption: A Comparative Lifecycle Assessment. *Energy* **2016**, *106*, 87–102. [CrossRef]
6. Heinzl, G.C.; Mota, D.A.; Martinis, V.; Martins, A.S.; Soares, C.M.F.; Osório, N.; Gominho, J.; Madhavan Nampoothiri, K.; Sukumaran, R.K.; Pereira, H.; et al. Integrated Bioprocess for Structured Lipids, Emulsifiers and Biodiesel Production Using Crude Acidic Olive Pomace Oils. *Bioresour. Technol.* **2022**, *346*, 126646. [CrossRef]
7. Mehdi, R.; Naqvi, S.R.; Khan, A.A.; Mirani, A.A. Optimization of Olive Oil Extraction from Olive Pomace Using Solvent Extraction and Response Surface Methodology Analysis of Oil Yield. *Fuel* **2023**, *348*, 128633. [CrossRef]
8. Lama-Muñoz, A.; Álvarez-Mateos, P.; Rodríguez-Gutiérrez, G.; Durán-Barrantes, M.M.; Fernández-Bolaños, J. Biodiesel Production from Olive–Pomace Oil of Steam-Treated Alperujo. *Biomass Bioenergy* **2014**, *67*, 443–450. [CrossRef]

9. Ayadi, M.; Awad, S.; Villot, A.; Abderrabba, M.; Tazerout, M. Heterogeneous Acid Catalyst Preparation from Olive Pomace and Its Use for Olive Pomace Oil Esterification. *Renew. Energy* **2021**, *165*, 1–13. [CrossRef]
10. Ayadi, M.; Saragih, F.N.A.; Awad, S.; Priadi, C.; Abderrabba, M.; Tazerout, M.; Andres, Y. Two Steps Methanolysis and Ethanolysis of Olive Pomace Oil Using Olive-Pomace-Based Heterogeneous Acid Catalyst. *Fuel* **2021**, *296*, 120678. [CrossRef]
11. Yücel, Y. Biodiesel Production from Pomace Oil by Using Lipase Immobilized onto Olive Pomace. *Bioresour. Technol.* **2011**, *102*, 3977–3980. [CrossRef]
12. López, I.; Quintana, C.E.; Ruiz, J.J.; Cruz-Peragón, F.; Dorado, M.P. Effect of the Use of Olive–Pomace Oil Biodiesel/Diesel Fuel Blends in a Compression Ignition Engine: Preliminary Exergy Analysis. *Energy Convers. Manag.* **2014**, *85*, 227–233. [CrossRef]
13. Redel-Macías, M.D.; Pinzi, S.; Leiva, D.; Cubero-Atienza, A.J.; Dorado, M.P. Air and Noise Pollution of a Diesel Engine Fueled with Olive Pomace Oil Methyl Ester and Petrodiesel Blends. *Fuel* **2012**, *95*, 615–621. [CrossRef]
14. Redel-Macías, M.D.; Pinzi, S.; Ruz, M.F.; Cubero-Atienza, A.J.; Dorado, M.P. Biodiesel from Saturated and Monounsaturated Fatty Acid Methyl Esters and Their Influence over Noise and Air Pollution. *Fuel* **2012**, *97*, 751–756. [CrossRef]
15. López, I.; Pinzi, S.; Leiva-Candia, D.; Dorado, M.P. Multiple Response Optimization to Reduce Exhaust Emissions and Fuel Consumption of a Diesel Engine Fueled with Olive Pomace Oil Methyl Ester/Diesel Fuel Blends. *Energy* **2016**, *117*, 398–404. [CrossRef]
16. Bereczky, Á.; Lukács, K.; Farkas, M.; Dóbé, S. Effect of γ-Valerolactone Blending on Engine Performance, Combustion Characteristics and Exhaust Emissions in a Diesel Engine. *Nat. Resour.* **2014**, *5*, 177–191. [CrossRef]
17. Çaynak, S.; Gürü, M.; Biçer, A.; Keskin, A.; İçingür, Y. Biodiesel Production from Pomace Oil and Improvement of Its Properties with Synthetic Manganese Additive. *Fuel* **2009**, *88*, 534–538. [CrossRef]
18. Kannan, G.R.; Karvembu, R.; Anand, R. Effect of Metal Based Additive on Performance Emission and Combustion Characteristics of Diesel Engine Fuelled with Biodiesel. *Appl. Energy* **2011**, *88*, 3694–3703. [CrossRef]
19. Zhen, D.; Song, Z.; Shi, Z.; Gu, F.; Ball, A. Combustion Noise Analysis for Combustion and Fuels Diagnosis of a Compression Ignition Diesel Engine Operating with Biodiesels. *Combust. Sci. Technol.* **2015**, *187*, 1974–1992. [CrossRef]
20. Khan, S.; Dewang, Y.; Raghuwanshi, J.; Shrivastava, A.; Sharma, V. Nanoparticles as Fuel Additive for Improving Performance and Reducing Exhaust Emissions of Internal Combustion Engines. *Int. J. Environ. Anal. Chem.* **2022**, *102*, 319–341. [CrossRef]
21. Gündüz, İ.; Oflaz, F.; Gürgenç, T. Comparative Effects of B_4C and h-BN Nanoparticles on the Performance and Emissions of a Diesel Engine Fueled with a Rapeseed Biodiesel Blend. *Sci. Rep.* **2026**. [CrossRef]
22. Ghanbari, M.; Najafi, G.; Ghobadian, B.; Yusaf, T.; Carlucci, A.P.; Kiani Deh Kiani, M. Performance and Emission Characteristics of a CI Engine Using Nano Particles Additives in Biodiesel-Diesel Blends and Modeling with GP Approach. *Fuel* **2017**, *202*, 699–716. [CrossRef]
23. El-Seesy, A.I.; Hassan, H.; Ookawara, S. Effects of Graphene Nanoplatelet Addition to Jatropha Biodiesel–Diesel Mixture on the Performance and Emission Characteristics of a Diesel Engine. *Energy* **2018**, *147*, 1129–1152. [CrossRef]
24. Sekhar, P.C.; Gupta, A.V.S.S.K.S. Diesel-Biodiesel Blends Using Nanoparticles with Dispersants: Combustion, Performance, and Emissions Analysis. *Next Mater.* **2025**, *9*, 101146. [CrossRef]
25. Gad, M.S.; Abdel Aziz, M.M.; Kayed, H. Performance, Emissions and Exergy Analyses of Adding CNTs to Various Biodiesel Feedstocks. *Propuls. Power Res.* **2022**, *11*, 511–526. [CrossRef]
26. Wu, Q.; Xie, X.; Wang, Y.; Roskilly, T. Effect of Carbon Coated Aluminum Nanoparticles as Additive to Biodiesel-Diesel Blends on Performance and Emission Characteristics of Diesel Engine. *Appl. Energy* **2018**, *221*, 597–604. [CrossRef]
27. Savaş, A.; Uslu, S.; Şener, R. Optimization of Performance and Emission Characteristics of a Diesel Engine Fueled with $MgCO_3$ Nanoparticle Doped Second Generation Biodiesel from Jojoba by Using Response Surface Methodology (RSM). *Fuel* **2025**, *381*, 133658. [CrossRef]
28. Haq, M.U.; Jafry, A.T.; Khan, W.U. Addition of Barium Titanate ($BaTiO_3$) and Molybdenum Disulfide (MoS_2) Nanoparticles to Castor Biodiesel for Diesel Engine Application. *J. Therm. Anal. Calorim.* **2025**, *150*, 11227–11246. [CrossRef]
29. Canan, A.; Çalhan, R.; Uslu, S. Green Fuel Innovation for Renewable Energy: Engine Response Optimization of $BaTiO_3$-Modified Spirulina Microalgae Biodiesel (3rd Generation)—Diesel Blends with RSM. *Renew. Energy* **2026**, *261*, 125331. [CrossRef]
30. Khan, I.; Saeed, K.; Khan, I. Nanoparticles: Properties, Applications and Toxicities. *Arab. J. Chem.* **2019**, *12*, 908–931. [CrossRef]
31. Hackley, V.A. *Measuring the Size of Nanoparticles in Aqueous Media Using Batch-Mode Dynamic Light Scattering*; NIST SP 1200-6; National Institute of Standards and Technology: Gaithersburg, MD, USA, 2015. [CrossRef]
32. Allasi, H.L.; Selvam, A.J.; Soosaimariyan, M.V.; Arul, S.J. Enhancing Diesel Engine Efficiency with Waste Cooking Oil Biodiesel and Nano Additives for Sustainable Fuel Applications. *Sci. Rep.* **2025**, *15*, 31762. [CrossRef]
33. Savaş, A.; Uslu, S.; Der, O.; Uslu, G.; Şener, R. Towards Sustainable Internal Combustion Engines: Optimization of Cobalt Oxide Nano-Additive Microalgae Biodiesel Blends for Emission Mitigation and Performance Enhancement. *Fire* **2026**, *9*, 250. [CrossRef]
34. Patel, D.; Azam, S.M.F.; Rao, P.S.R.; Chohan, J.S.; Singh, R.; Samantaray, S.; Thykattusserry, N.J.; Bisht, Y.S.; Bhowmik, A.; Tamene, Y. Experimental Investigation of ZnO Nanoparticle–Enhanced Pongamia Biodiesel for Performance, Combustion, Emission, and Sustainability Assessment in a CI Engine. *Sci. Rep.* **2026**, *16*, 23264. [CrossRef]

35. Sabapathy, S.P.; Ammasi, A.M.; Khalife, E.; Babu, M.; Munusamy, S.; Sabapathy, P.; Gharehghani, A.; Szymanek, M.; Kaveh, M. Optimization of Injection Timing and Ethyl Hexyl Nitrate Additive Effects on Diesel Engine Characteristics Using Rubber Seed Oil Biodiesel. *Int. J. Energy Res.* **2025**, *2025*, 1686933. [CrossRef]
36. Filon, D.; Anastopoulos, G.; Karonis, D. Synthesis and Evaluation of Bio-Lubricants from Renewable Raw Materials. *Lubricants* **2024**, *12*, 446. [CrossRef]
37. Selaimia, R.; Beghiel, A.; Oumeddour, R. The Synthesis of Biodiesel from Vegetable Oil. *Procedia-Soc. Behav. Sci.* **2015**, *195*, 1633–1638. [CrossRef]
38. Moffat, R.J. Describing the Uncertainties in Experimental Results. *Exp. Therm. Fluid Sci.* **1988**, *1*, 3–17. [CrossRef]
39. Raman, L.A.; Deepanraj, B.; Rajakumar, S.; Sivasubramanian, V. Experimental Investigation on Performance, Combustion and Emission Analysis of a Direct Injection Diesel Engine Fuelled with Rapeseed Oil Biodiesel. *Fuel* **2019**, *246*, 69–74. [CrossRef]
40. Fareed, A.F.; El-Shafay, A.S.; Gad, M.S.; Ağbulut, Ü. Experimental Assessment of Hybrid Binary and Ternary Fuel Blends on CI Engine Performance, Emissions, and Combustion Characteristics. *J. Therm. Anal. Calorim.* **2025**, *150*, 4695–4709. [CrossRef]
41. Gad, M.S.; Jayaraj, S. A Comparative Study on the Effect of Nano-Additives on the Performance and Emissions of a Diesel Engine Run on Jatropha Biodiesel. *Fuel* **2020**, *267*, 117168. [CrossRef]
42. Devarajan, Y.; Nagappan, B.; Subbiah, G. A Comprehensive Study on Emission and Performance Characteristics of a Diesel Engine Fueled with Nanoparticle-Blended Biodiesel. *Environ. Sci. Pollut. Res.* **2019**, *26*, 10662–10672. [CrossRef]
43. Gad, M.S.; Ağbulut, Ü.; Afzal, A.; Panchal, H.; Jayaraj, S.; Qasem, N.A.A.; El-Shafay, A.S. A Comprehensive Review on the Usage of the Nano-Sized Particles along with Diesel/Biofuel Blends and Their Impacts on Engine Behaviors. *Fuel* **2023**, *339*, 127364. [CrossRef]
44. Rahman, M.A.; Hasnain, S.M.M.; Pandey, S.; Tapalova, A.; Akylbekov, N.; Zairov, R. Review on Nanofluids: Preparation, Properties, Stability, and Thermal Performance Augmentation in Heat Transfer Applications. *ACS Omega* **2024**, *9*, 32328–32349. [CrossRef]
45. Janaki, V.; Ranjit, P.S.; Balakrishna, B. Performance Emission and Combustion Characteristics of TIO_2 and CEO_2 Nanoparticle Enhanced Mahua Biodiesel Diesel Blends Using Experimental and Machine Learning Approaches. *Sci. Rep.* **2026**, *16*, 8594. [CrossRef]
46. Channapattana, S.V.; Campli, S.; Madhusudhan, A.; Notla, S.; Arkerimath, R.; Tripathi, M.K. Energy Analysis of DI-CI Engine with Nickel Oxide Nanoparticle Added Azadirachta Indica Biofuel at Different Static Injection Timing Based on Exergy. *Energy* **2023**, *267*, 126622. [CrossRef]
47. Gollamudi, A.A.; Koka, N.S.S.; Bhatti, S.K.; Sagari, J. Vibration and Noise of Diesel Engine Using Calophyllum Inophyllum Biodiesel and MoO_3 Nanoparticles: Experimental and Machine Learning Study. *Int. J. Thermofluids* **2024**, *24*, 100925. [CrossRef]
48. Sethin, A.; Oo, Y.M.; Thawornprasert, J.; Somnuk, K. Effects of Blended Diesel–Biodiesel Fuel on Emissions of a Common Rail Direct Injection Diesel Engine with Different Exhaust Gas Recirculation Rates. *ACS Omega* **2024**, *9*, 20906–20918. [CrossRef]
49. Prabu, A. Nanoparticles as Additive in Biodiesel on the Working Characteristics of a DI Diesel Engine. *Ain Shams Eng. J.* **2018**, *9*, 2343–2349. [CrossRef]
50. Pullagura, G.; Bikkavolu, J.R.; Vadapalli, S.; Siva Prasad, V.V.; Rao Chebattina, K.R.; Barik, D.; Dennison, M.S. Performance, Combustion and Emission Reduction Characteristics of Metal-Based Silicon Dioxide Nanoparticle Additives Included in Ternary Fuel (Diesel-SMME-Iso Butanol) on Diesel Engine. *Heliyon* **2024**, *10*, e26519. [CrossRef]
51. Torkzaban, S.; Feyzi, M.; Norouzi, L. A Novel Biodegradable Nanoparticle as a Robust Biodiesel Antioxidant, and Fuel Additive for Improvement of Diesel Engine Performance and Exhaust Emission. *Renew. Energy* **2025**, *242*, 122345. [CrossRef]
52. Balasubramanian, D.; Hoang, A.T.; Papla Venugopal, I.; Shanmugam, A.; Gao, J.; Wongwuttanasatian, T. Numerical and Experimental Evaluation on the Pooled Effect of Waste Cooking Oil Biodiesel/Diesel Blends and Exhaust Gas Recirculation in a Twin-Cylinder Diesel Engine. *Fuel* **2021**, *287*, 119815. [CrossRef]
53. Gamboa, D.; Herrera, B.; Acevedo, J.; López, D.; Cacua, K. Experimental Evaluation of a Diesel Engine Using Amide-Functionalized Carbon Nanotubes as Additives in Commercial Diesel and Palm-Oil Biodiesel. *Int. J. Thermofluids* **2024**, *22*, 100669. [CrossRef]
54. Khujamberdiev, R.; Cho, H.M. Evaluation of TiO_2 Nanoparticle-Enhanced Palm and Soybean Biodiesel Blends for Emission Mitigation and Improved Combustion Efficiency. *Nanomaterials* **2024**, *14*, 1570. [CrossRef]
55. Lavoie, G.A.; Heywood, J.B.; Keck, J.C. Experimental and Theoretical Study of Nitric Oxide Formation in Internal Combustion Engines. *Combust. Sci. Technol.* **1970**, *1*, 313–326. [CrossRef]
56. Mueller, C.J.; Boehman, A.L.; Martin, G.C. An Experimental Investigation of the Origin of Increased NO_x Emissions When Fueling a Heavy-Duty Compression-Ignition Engine with Soy Biodiesel. *SAE Int. J. Fuels Lubr.* **2009**, *02*, 789–816. [CrossRef]
57. Hong, T.; Brinkman, K.S.; Xia, C. Barium Carbonate Nanoparticles as Synergistic Catalysts for the Oxygen Reduction Reaction on $La_{0.6}Sr_{0.4}Co_{0.2}Fe_{0.8}O_{3-\delta}$ Solid-Oxide Fuel Cell Cathodes. *ChemElectroChem* **2016**, *3*, 805–813. [CrossRef]
58. Basu, T.K.; Searcy, A.W. Kinetics and Thermodynamics of Decomposition of Barium Carbonate. *J. Chem. Soc. Faraday Trans. 1 Phys. Chem. Condens. Phases* **1976**, *72*, 1889. [CrossRef]
59. Venu, H.; Subramani, L.; Raju, V.D. Emission Reduction in a DI Diesel Engine Using Exhaust Gas Recirculation (EGR) of Palm Biodiesel Blended with TiO_2 Nano Additives. *Renew. Energy* **2019**, *140*, 245–263. [CrossRef]

60. Guo, Z.; Wu, C.-W.; Wu, Y.-L.; Lee, Y.-Y.; Lin, S.-L.; Lee, T.H. Spray Combustion Characteristics and Soot Formation Potential of Nano-Al_2O_3 Diesel at Low Ambient Temperatures. *Fuel* **2024**, *371*, 132086. [CrossRef]
61. Jain, A.; Ambekar, A.; Thajudeen, T. Effect of Titania Nano-Additives on Fine and Ultrafine Carbonaceous Emissions during Flame Combustion of Diesel. *Aerosol Air Qual. Res.* **2024**, *24*, 230281. [CrossRef]
62. Gallego, A.; Lapuerta, M.; Hernández, J.J.; Gómez, D.; Herrera, B.; Cacua, K. Technical Feasibility Analysis of Carbon Nanotubes in Diesel Engines: Effects on Stability, Combustion Properties and Emissions. *Energy Convers. Manag.* **2025**, *326*, 119450. [CrossRef]
63. Özer, S.; Demir, U.; Koçyiğit, S. Effect of Using Borax Decahydrate as Nanomaterials Additive Diesel Fuel on Diesel Engine Performance and Emissions. *Energy* **2023**, *266*, 126412. [CrossRef]
64. Ağbulut, Ü.; Sarıdemir, S. Synergistic Effects of Hybrid Nanoparticles along with Conventional Fuel on Engine Performance, Combustion, and Environmental Characteristics. *Energy* **2024**, *292*, 130267. [CrossRef]
65. Kumar, N.; Raheman, H. Production, Characterization and Utilization of Second Generation Biodiesel Blend in Diesel Engine Using Water and Nanoparticles as Additives. *Fuel* **2022**, *308*, 122063. [CrossRef]

Disclaimer/Publisher's Note: The statements, opinions and data contained in all publications are solely those of the individual author(s) and contributor(s) and not of MDPI and/or the editor(s). MDPI and/or the editor(s) disclaim responsibility for any injury to people or property resulting from any ideas, methods, instructions or products referred to in the content.